Control of dissipation sources: A central aspect for enhancing the mechanical and mechanobiological performances of hydrogels

Naser Nasrollahzadeh, Peyman Karami, Dominique P. Pioletti*.

Laboratory of Biomechanical Orthopedics, Institute of Bioengineering, EPFL, 1015 Lausanne, Switzerland.

KEYWORD: Hydrogel, sources of dissipation, fatigue resistance, cartilage, mechanobiology.

ABSTRACT: Development of mechanically durable and biologically inductive hydrogels is a major challenge for load-bearing applications such as engineered cartilage. Dissipative capacity of articular cartilage is central to its functional behavior when submitted to loading. While fluid frictional drag is playing a significant role in this phenomenon, the flow-dependent source of dissipation is mostly overlooked in the design of hydrogel scaffolds. Herein, we propose an original strategy based on the combination of fluidic and polymeric dissipation sources to simultaneously enhance hydrogels mechanical and mechanobiological performances. The non-destructive dissipation processes were carefully designed by hybrid crosslinking of the hydrogels network and low permeability of the porous structure. It was found that intra-chains and pores water distribution in the porous hydrogels improves the mechanical properties in high water fractions. In contrast to widely reported tough hydrogels presenting limited load support capability at low strain values, we obtained stiff and dissipative

20   hydrogels with unique fatigue behavior. We showed that the fatigue resistance capability is not

21   a function of morphology, dissipation level, and stiffness of the hydrogels but rather depends

22   on the origin of the dissipation. Moreover, the preserved dissipation source under mechanical

23   stimulation maintained a mechano-inductive niche for enhancing chondrogenesis thanks to

24   fluid frictional drag contribution. The proposed strategy can be widely used to design

25   functional scaffolds in high loading demands for enduring physiological stimuli and generating

26   regulatory cues to cells.

1   INTRODUCTION

28   Engineering functional hydrogels presenting cells promoting features and robust fatigue

29   behavior is a significant challenge in the biomaterial field, particularly for load-bearing tissues

30   like cartilage. [1-3] Viscoelasticity of cartilage tissue is central to its functional behavior and

31   homeostasis in the demanding biomechanical condition of synovial joints.[4-6] From a biological

32   point of view, evidence is now growing that cells fate can be regulated by viscoelasticity of

33   their surrounding microenvironment in three dimensional hydrogels.[6-9] From a mechanical

34   standpoint, energy dissipation (ED) is an essential viscoelastic property for a load-bearing

35   material to damp the input energy and avoid failure. [10-11] Preserved dissipation is thus a key

36   characteristic for long term and durable performance of biomaterials under fatigue loading.

37   Design of proper dissipative sources for hydrogel scaffolds could therefore be a strategic

38   approach to simultaneously improve their mechanical and mechanobiological performances.

39   The level of ED is quantified by the area of hysteresis loop when the material is under cyclic

40   mechanical loading. While mechanical dissipation is generally described as a global variable,

41   the specific origin of dissipation could highly impact the hydrogels functionality. The energy

42   dissipation of a biphasic material arises from fluid frictional drag force and intrinsic

43   viscoelasticity of the solid matrix following reversible or/and irreversible processes. Various

44   dissipative hydrogels have been developed based on different molecular structures to modulate

45   polymeric dissipation sources. In this intensive research context, innovative strategies were

46   proposed including double network,[12-13] hydrophobic modification,[14] block copolymers,[15]

47   opposite polyelectrolytes,[16] as well as hybrid,[17] and composite,[18] systems. They all follow the

48   same principle of dissipating the imposed input energy by incorporating sacrificial elements

49   into the polymeric network. [10] Moreover, considerable efforts have been devoted to the

50   development of dissipative hydrogels with the aim of achieving toughness of biological tissues

51   to sustain physiological loads. [3, 13, 19] However, insufficient load support capability in moderate

52   strain range often limits the application of these tough hydrogels especially for cartilage tissue

53   regeneration. In addition, a merely stiff and dissipative hydrogel does not necessarily present a

54   fatigue resistance capability. Accordingly, dissipation sources of reversible nature have been

55   recently considered for a robust mechanical behavior.[19-22] Despite development of a few

56   dissipative hydrogels with appropriate stiffness, the lack of chemical stability,[15, 23] low water

57   content,[16, 24-25] and long recovery time after loading,[16-17, 23-24] still hamper their application.

58   We hypothesize that one key aspect for a durable performance of load-bearing hydrogels

59   under cyclic loading is a careful and smart design of their dissipative sources. While fluid

60   frictional drag is critical for biomechanical behavior of cartilage tissue, [4-5] this flow-dependent

61   source of dissipation is usually overlooked in dissipative hydrogels with intrinsic dissipation

62   sources.[10, 26] Indeed, the fluid-solid interaction source of dissipation is controllable through a

63   modulation of the biphasic structures permeability. [27-28] Accordingly, the flow-independent

64   sources of dissipation can be supplemented with flow-dependent mechanisms to obtain a load-

65   bearing hydrogel with fatigue resistance characteristic. In parallel, analysis of cells-scaffold

66   interaction to different dissipation sources can provide new insights on the role of viscoelastic

67   phenomenon on cells behavior. We therefore propose a novel strategy based on the control of

68   dissipation sources to design hydrogels with robust mechanical behavior and enhanced

69   mechanobiological feature.

Herein, we report that by an original combination of flow-dependent and flow-independent dissipation sources, fatigue resistant hydrogels can be developed with similar range of compressive stiffness, dissipation and water content to cartilage. For this purpose, hydrogel's composition-permeability pair is introduced to manipulate the network intrinsic dissipation and fluid frictional drag sources. Accordingly, the influence of material composition on flow-independent dissipation source is firstly analyzed in conventional hydrogels. Then, the design of porous hydrogels with tunable permeability is proposed to modulate flow-dependent source of dissipation. We also show that hydrogels having preserved hysteresis sources are fatigue resistance regardless of their stiffness and dissipation level. Finally, the enhanced mechanical behavior, obtained by controlling the dissipation origins, is further applied to the mechanobiological response of cells-laden porous hydrogels. In particular, chondrogenesis is favored during mechanical stimulation in fatigue resistant hydrogels having effective contribution of frictional drag mechanism. Collectively, we address how the design of the different dissipation sources opens the possibility to develop functional hydrogels with enhanced mechanical and biological performances.

2   EXPERIMENTAL SECTION

2.1   Hydrogels Fabrication

We used [2-hydroxyethyl methacrylate] (HEMA) as the main monomer for the polymeric network and ethylene glycol dimethacrylate (EGDMA) as the covalent crosslinker. Precursors of conventional poly HEMA based hydrogels were prepared with different concentrations of EGDMA and bi-distillated water. By adding the 2,2-dimethoxy-2-phenylacetophenone (DPAP- 0.1% of mol HEMA) photo-initiator, the solution was transferred to cylindrical transparent molds (6 mm diameter and 2.5 mm thickness) and covered with narrow microscope glass. After UV polymerization for 15 min (365 nm & 2 mW/cm^2), as-prepared conventional hydrogels were used for swelling study. We name the hydrogel prepared this way as

4

"conventional hydrogel" as opposed to "porous hydrogel" described below. The conventional pHEMA based hydrogels are referred to xCr-yW, where x and y stand respectively for EGDMA molar and initial water content volumetric ratios (%) to HEMA (Cr and W are abbreviations for crosslinking and water).

Salt leaching method was employed for porous hydrogels fabrication following UV radiation or heat polymerization (details in supporting information). Briefly, DPAP or redox pair (ammonium persulfate and sodium metabisulfite) as initiating agent was mixed with HEMA-EGDMA solution for UV or heat polymerization (Figure S3), respectively. The hydrogel precursor was then added to the sieved salt particles inside cylindrical Teflon molds (Table S2). To remove entrapped salt particles and allow swelling of the polymeric network, samples were kept in stirred water for one week during which the water was changed regularly. The diameter and thickness of the hydrated porous hydrogels were sized using a punch and home-made cutting tool (8 mm diameter, 2.5 mm height). The porous pHEMA hydrogels are defined with xCr-size configuration, where x stands for EGDMA molar ratio (%) to HEMA, and size represents the size of the meso pores (extra fine, fine, medium, and coarse).

2.2 Hydrogels Characterization

The volumetric swelling ratio of the conventional hydrogels was calculated according to Equation 1 by measuring the samples volume using a density determination kit (Density Kit MS-DNY-43, Mettler Toledo, USA). For this purpose, as prepared and swollen hydrogels were weighed in air (W_{air}) and when submerged in ethanol ($W_{eth.}$) and their corresponding volume was calculated by Equation 2 based on Archimedes' buoyancy principle.[29-30] Similarly, the equilibrium water content (EWC) of the hydrogels (either conventional or porous) was determined via the volume of the hydrated ($W_{air}^{swollen}$) and weight of the dried (W_{dried}) samples according to Equation 3.

5

$$Q_v = \frac{V_{swollen}}{V_{as\ prepared}} \tag{1}$$

$$V = \frac{(W_{air} - W_{eth.})}{\rho_{ethanol}} \tag{2}$$

$$EWC = \frac{(W_{air}^{swollen} - W_{dried})/\rho_{H2O}}{V_{swollen}} \tag{3}$$

119   Micro-computed tomography (μCT Skyscan 1176, Bruker, Kontich, Belgium) scans of

120   freeze-dried samples were employed for the morphological analysis. Pores distribution was

121   evaluated by CTAn software (Bruker) and 3D images were created by AMIRA software (FEI

122   Visualization Sciences Group, Burlington, MA, USA) using reconstructed μCT scans. The

123   strain-dependent permeability (k(ε)) of the porous hydrogels was determined based on Darcy's

124   law by using our custom-build rig described elsewhere. [27] Briefly, the flow rate was measured

125   under constant water head condition by measuring the weight of traversing water through the

126   porous hydrogels in a period of time.

127   Once hydrogel disks equilibrated in water, force-displacement data was collected during

128   cyclic compression of samples in a water bath by Instron machine (E3000, Norwood,

129   Massachusetts, USA) to quantify energy dissipation level. Initial cross section area and

130   thickness of samples were used to calculate stress-strain values from raw load-displacement

131   data. Three sequential unconfined compressions and hold steps were applied on samples

132   immersed in water to evaluate time dependent load support over stress relaxation test.

133   Additionally, we employed corresponding relaxed stress and strain values to calculate the slope

134   of the best linear fit as equilibrium Young modulus (Eeq.). As fatigue resistance metrics, we

135   evaluated i) the load support capability of hydrogels before and after one hour fatigue loading

136   (3600 cycles) and ii) the differential value of the energy dissipation (ΔED) normalized by the

137   energy dissipation of a reference cycle according to Equation 4. The ΔED was calculated by

138   subtraction of the latter cycle from the former cycle and an intermediate cycle number (cycle

139   100) was considered as the reference ED for normalizing the ΔED between cycles 10, 100 and

140   1000.

$$\frac{\Delta\text{ED}}{ED_{ref}} = \frac{ED_i - ED_{ref}}{ED_{ref}} \ if \ i < ref \ \& \ \frac{\Delta\text{ED}}{ED_{ref}} = \frac{ED_{ref} - ED_i}{ED_{ref}} \ if \ i > ref \qquad (4)$$

141   A poro-viscoelastic model,[31] of porous hydrogels was developed using COMSOL

142   Multiphysics (COMSOL Inc., Burlington, MA, USA) by employing Darcy's Law and Solid

143   Mechanics modules. The solid and the fluid phases were coupled based on theory of poro-

144   elasticity,[32] and a linear viscoelastic behavior for the solid part was assumed according to

145   Maxwell–Wiechert model. [33] To minimizes the error of the simulation and experimental data,

146   an estimation routine based on particle swarm optimization,[34] was defined for finding the best

147   set of parameters for network viscoelasticity. The optimized finite element model was then

148   used to separate the flow-dependent and the flow-independent viscoelasticity of the porous

149   hydrogels thanks to direct characterization of permeability. A complete description of the

150   methods used for experimental and computational characterization of hydrogels can be found

151   in supporting information.

152   **2.3   Mechanobiological Study**

153   Human epiphyseal chondro-progenitor cells were expanded in 2D culture according to

154   established cell culture protocols.[35] Porous hydrogels were sterilized and coated with

155   fibronectin before the cell seeding step for the sake of bioactivity and inducing similar cell-

156   hydrogel interface in different groups of study. [6,36] Cells infusion into porous hydrogels was

157   carried out by an optimized compression released induced suction (CRIS) method as described

158   in our previous work.[36] Hydrogels were then pre-cultured for 3 days in proliferation medium

159   inside a standard incubator (37°C, 5% CO_2). After this step, differentiation medium was used

160   and starting from day 5, the mechanical stimulation was applied on porous hydrogels using a

161   home-made bioreactor. [6] The stimulation time was 2 hours per day for a period of 4 days, while

162   the corresponding control groups were incubated in equivalent condition but without

163   mechanical loading. Detail process of mechanobiological experiment and analysis can be found

164   in supporting information (Figure S12-a and Table S4).

165   **2.4   Statistical analysis**

166   The extracted results were reported by mean and standard deviation values for mechanical

167   properties and average, maximum and minimum fold changes for gene expression data. The

168   statistical significance between different study groups was determined by Student t-test when

169   required (n=4).

170   **3   RESULTS AND DISCUSSION**

171   **3.1   Conventional hydrogels with intrinsic dissipation sources**

172   By following the sacrificial bonds principle,[15-16, 26] a fatigue-resistant single network hydrogel

173   can be developed via a hybrid crosslinking strategy.[10] We therefore used biocompatible HEMA

174   polymer to design a hybridly crosslinked single network hydrogel. Different physical bonds

175   can be formed within pHEMA network thanks to the available functional groups of the chains.

176   Furthermore, the stiffness and the dissipation level of pHEMA hydrogels can be significantly

177   enhanced if the network is copolymerized by a covalent crosslinker (Cr). [37] We developed 5

178   groups of conventional pHEMA based hydrogels and evaluated the role of material

179   composition in bonds formation and resultant mechanical properties. The contribution of weak

180   and strong bonds to the mechanisms of intrinsic network dissipation and fatigue performance

181   was then analyzed.

182   The mechanical properties of the conventional pHEMA hydrogels could be modulated via

183   their polymeric composition as shown in Figure 1. We observed softer hydrogels in higher

184   water contents (e.g., 3Cr-50W vs. 3Cr-55W) confirming the inverse correlation between void

185   space and the stiffness of biomaterials. [38] In parallel, the higher covalent crosslinking ratio

186   provides a stiffer and more dissipative hydrogel (Figure 1-a) with the same water content.

8

Regardless of the level of dissipation and stiffness, the dissipation origin should be reversible and non-destructive for a fatigue resistant material. While hysteresis loop in hydrogels with destructive dissipation is shrinking over cyclic loadings, fatigue resistant hydrogels preserve their dissipative capacity. Representative hysteresis loops evolution and load support capability of hydrogels with (4Cr-55W) and without (7Cr-60W) fatigue resistance characteristic are illustrated in Figure 1-b and Figure S1. The 7Cr-60W hydrogel shows the highest ED reduction over cyclic compression (Figure 1-c) despite its lower stiffness than other hydrogels. Conversely, the 4Cr-55W hydrogel presents a fairly stiff and dissipative hydrogel with a robust fatigue performance thanks to its non-destructive dissipation source. We also compared the tensile properties of the hydrogels as shown in Figure S2. In general, the tensile tests confirmed the results of compressive loading regime in different groups of hydrogels (e.g., similar trends for modulus, dissipative capacity and fatigue performance).
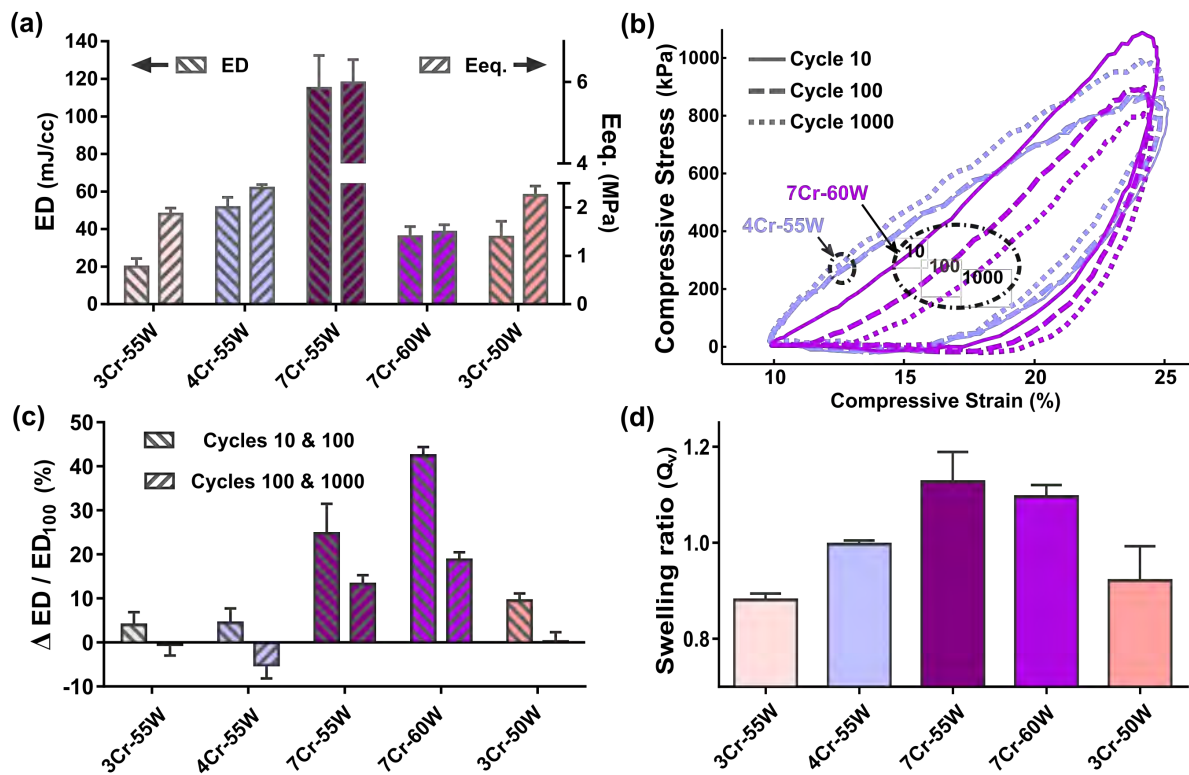
Figure 1. Single network pHEMA based hydrogels characteristics. (a) Energy dissipation per unit volume was obtained by applying 15% cyclic compression at 1 Hz over 10% static strain

202   (ED value is the average over the 90th to 100th loading cycles, left axis) and equilibrium

203   Young's modulus (Eeq. was measured between 10 to 20% compressive strains, right axis) of

204   the hydrogels. (b) Hysteresis loop evolution of 4Cr-55W (light blue) and 7Cr-60W (purple)

205   hydrogels during cyclic loading demonstrating the preserved and reduced energy dissipation

206   (ED) level, respectively. (c) The differential normalized value of the energy dissipation during

207   cyclic loading for cycle 10 and 1000 with respect to cycle 100 as the reference cycle ($\frac{\Delta ED}{ED_{100}}$)

208   where ΔED was calculated by subtraction of the latter cycle from the former cycle. (d)

209   Volumetric swelling ratio (Q_v) of the developed hydrogels.

210   Incorporation of recoverable sacrificial bonds to a flexible network ensures a durable

211   dissipative behavior following mechanical loadings.[10] A secondary structure is likely to form

212   by reversible physical bonds in pHEMA network with nano-mesh sizes (Table S1), provided

213   that the network flexibility and density allows it. The hydrophobic tendency of methyl (CH_3)

214   groups in pHEMA chain acts as a driving force to form hydrophobic associations within the

215   network.[39-40] In addition, polar hydroxyl (OH) and carbonyl (C=O) side chains in pHEMA not

216   only bring hydrophilicity to the network but also allow hydrogen bonding,[41-42] or intra-chains

217   sliding/interaction following deformation.[37] We verified the contribution of the physical bonds

218   to the hydrogels network by evaluating their volumetric swelling ratio (Figure 1-d) and fatigue

219   behavior. The 7Cr-55W hydrogel presented a mild swelling in water ($Q_v > 1$) meaning that the

220   hydrophilic tendency of the pHEMA chains in a constrained network overcame the chains

221   attraction force for physical bonds formation. Conversely, we observed de-swelling ($Q_v < 1$) for

222   the 3Cr-55W hydrogel indicating that the shrinking forces prevailed, thanks to the flexibility

223   of its network. In parallel, the normalized ED differences are higher for 7Cr-55W hydrogel

224   than 3Cr-55W hydrogel during cyclic loading (Figure 1-c), which presents a weaker fatigue

225   performance in a constrained network. In case of 4Cr-55W hydrogels, the swelling and

226   shrinking forces almost equilibrated ($Q_v \sim 1$), further supporting the inverse correlation between

227   network rigidity and physical bonds formation.

228   The significance of a careful design of polymeric network for obtaining a preserved and

229   adequate intrinsic dissipation source is schematically illustrated in Figure 2. A high density of

230   strong covalent bonds can over constrain the hydrogels network, reduce its resilience and

231   hamper formation of a secondary structure. Consequently, the network may either experience

232   chains fracture between two crosslinks or bonds rupture at the crosslinking location upon an

233   applied deformation as depicted in Figure 2-a. Both of these processes are highly dissipative,

234   nevertheless causing permanent and not recoverable damage even after a long recovery time

235   (Figure S1). Alternatively, a careful combination of physical and covalent bonds provides a

236   hybrid crosslinking system with fatigue resistance capability as schematically illustrated in

237   Figure 2-b. In such a hydrogel, the network is sparsely populated by the covalent bonds to

238   maintain stability of the system. The macromolecular configuration in this flexible network can

239   be reorganized upon deformation to dissipate energy by reversible dissociation of physical

240   bonds and polymeric chains rearrangement. Preserving high dissipative capacity with non-

241   destructive processes, however, can only be accomplished with an increased polymer fraction

242   (dense network) of the hydrogel. Indeed, a higher portion of free water between chains

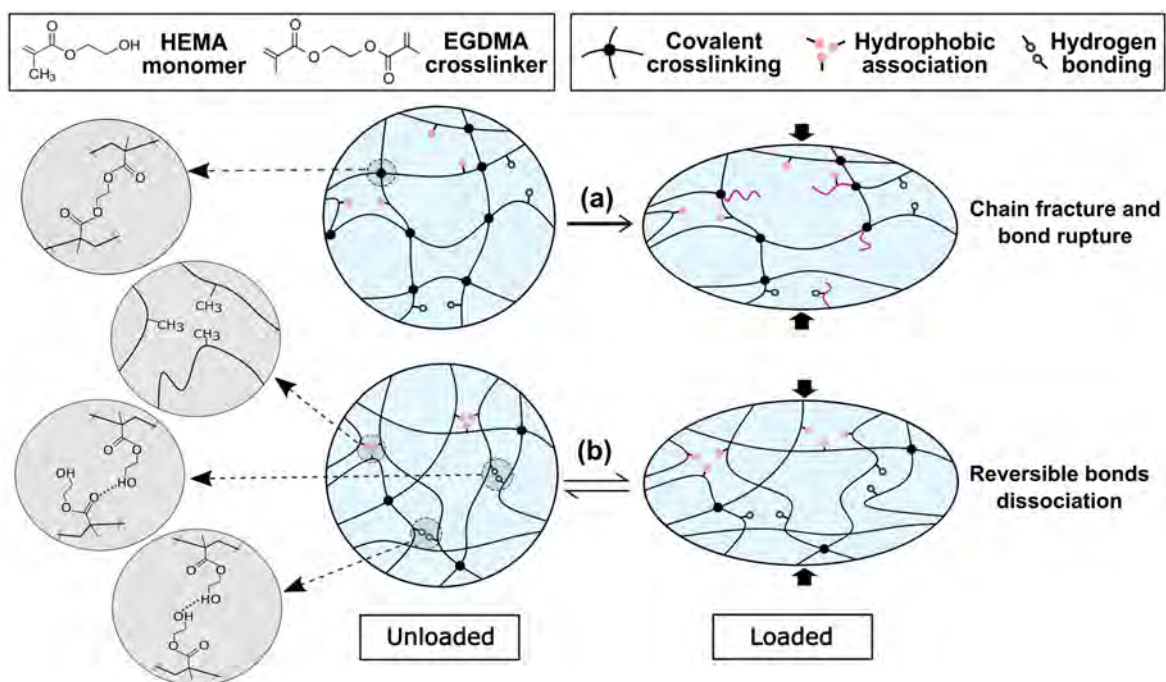243   diminishes the required sources for ED in the network by isolating the chains.

Figure 2. Influence of the macromolecular network of pHEMA based hydrogels on polymeric dissipation origin. (a) High concentration of covalent bonds leads to destructive dissipation upon an applied deformation. Following deformation of the constrained network, bonds rupture at the crosslinking location or chains fracture between two crosslinks (showed by purple color) could occur which are irreversible sources of dissipation. (b) Optimal hybrid crosslinking dissipates input energy non-destructively. Dissociation of physical bonds and chains rearrangement within the flexible network lead to reversible polymeric dissipation.

3.2 Porous hydrogels design

3.2.1 Water distribution in different length scales to enhance hydrogel mechanical properties

The stiffness and dissipative capacity of conventional pHEMA hydrogels significantly dropped (Table 1) with a water content range close to the cartilage (65-80%) [4-5]. Imposing a large amount of water in conventional pHEMA hydrogels loosens their networks and prevents adequate physical bonds formation.[42-43] It can also lead to polymerization induced phase

12

259   separation which forms elastically inactive chains within the network. [40] Indeed, the presence

260   of heterogeneous water compartments within hierarchical structure of load-bearing tissues

261   (intra and extra fibrillar fluids) optimizes their mechanical performance.[4,44] The patterned water

262   distribution in different length scales (e.g., nano meshes and meso pores) is, therefore, an

263   interesting strategy to design functional hydrogels. Accordingly, we developed porous

264   hydrogels with intra-chain and pore water fractions to maintain the mechanical functionality in

265   a physiological water content as shown in Figure 3. It was found that with a fluid phase in

266   cartilage range (~70%), stiffness and dissipative capacity of a porous pHEMA hydrogel are

267   significantly higher than corresponding conventional hydrogels (Table 1). Besides improved

268   mechanical properties in a relatively high water content, a great advantage of a porous hydrogel

269   design is the control over flow-dependent source of dissipation.

270   **Table 1.** Mechanical properties of conventional and porous pHEMA hydrogels (UV

271   polymerized) containing around 70% water corresponding to the cartilage physiological water

272   content.

Hydrogel	EWC (%)	ED (mJ/cc)	Eeq. (kPa)
3Cr-66W: conventional	68±1	5.5±0.51	148.05±9.17
3Cr-Ext. Fine: porous	69±1	12.55±0.72*	361.33±30.66*
4Cr-66W: conventional	67±1	7.51±1.03	293.75±54.58
4Cr-Ext. Fine: porous	69±1	14.52±1.11*	506.41±67.76*

EWC: Equilibrium water content.
ED: Energy dissipation (10% static+15% at 1 Hz).
Eeq.: Equilibrium Young's modulus (10-20% strain).

* Significant difference between porous and corresponding conventional groups ($p < 0.01$, n=4).
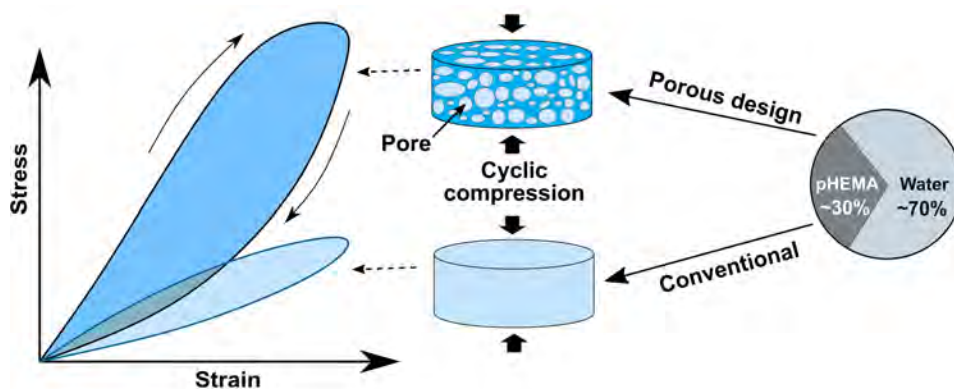
Figure 3. Influence of pHEMA based hydrogels fabrication methods on their mechanical

behavior in 70% water content condition. The patterned water distribution in different length

scales (pore and intra-chains water portions) leads to superior mechanical properties for porous

pHEMA hydrogels (obtained by salt-leaching) compared to conventionally prepared hydrogels

in high water fractions.

3.2.2 Modulating different origins of dissipation in porous hydrogels

A multi-mechanism dissipative design can be accomplished in porous hydrogels by

employing flow-dependent and flow-independent dissipation sources. The fluid flow and

accordingly frictional drag source of dissipation depend on the permeability in porous materials

such as articular cartilage.[45] Indeed, the permeability of porous hydrogels can be engineered by

their pore sizes while keeping the water fraction constant. [27] Accordingly, to modulate fluidic

and solid intrinsic dissipations, five groups of porous hydrogels were developed presenting

different pore sizes and Cr ratio as reported in Table S2. In these samples, the pores and intra-

chains water fractions occupy around 50% and 20% of the hydrogels total volume, respectively.

The morphological characteristics of the developed porous hydrogels are displayed in Figure

4. Significant decrease in the permeability of the hydrogels with smaller pores was confirmed

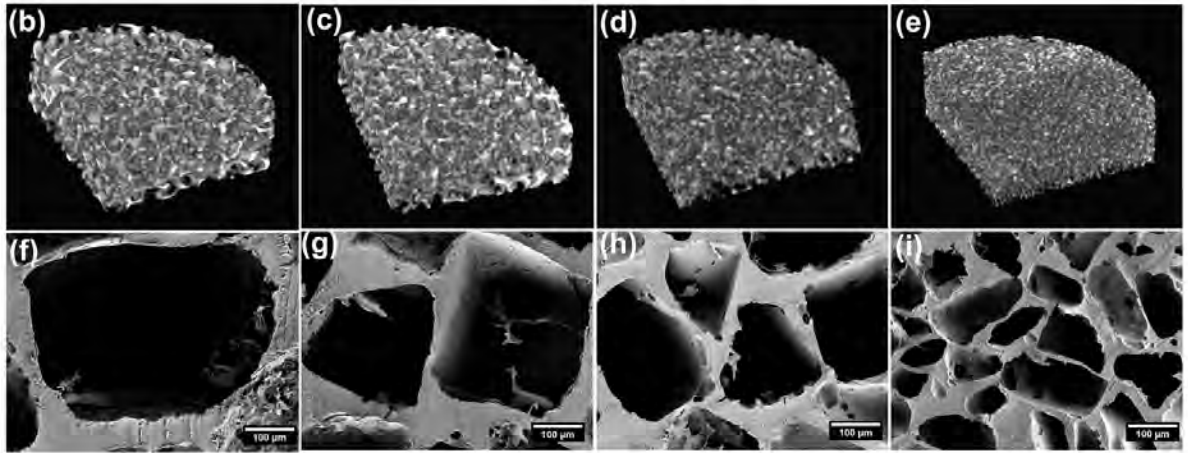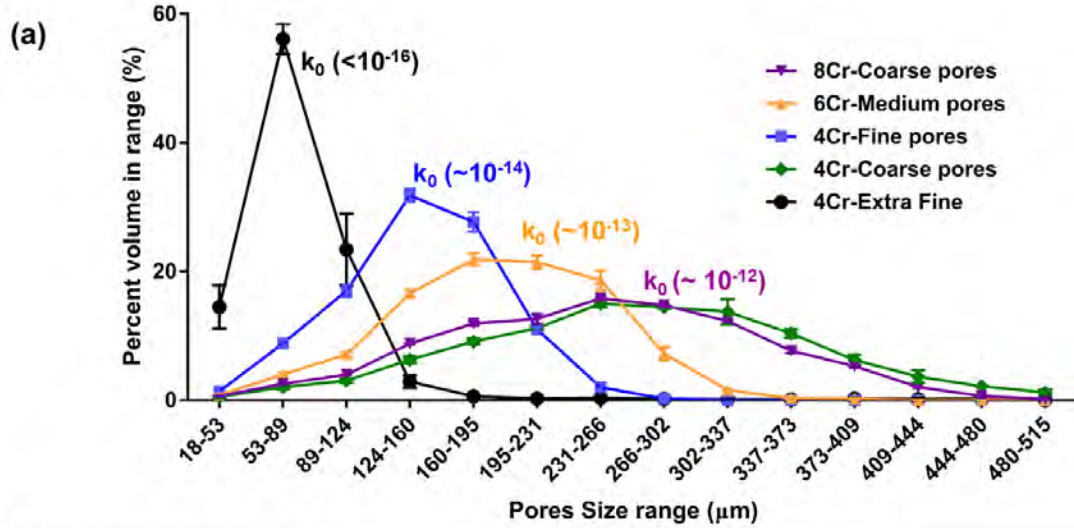with direct permeability measurements (Figure 4-a & Table S2).

14

Figure 4. Porous hydrogels morphological characteristics in the dried state. (a) Pores size distribution of the porous hydrogels determined by analysis of μCT scans and corresponding strain-free permeability (k_0: m^2). (b-e) Reconstructed 3D images using μCT scans for porous hydrogel having coarse, medium, fine, and extra fine pores, respectively. (f-i) SEM graphs of porous hydrogel having coarse, medium, fine, and extra fine pores, respectively (scale bar: 100 μm).

We found that the stiffness and dissipative capacity are indirectly related to the permeability and directly to the Cr ratio of porous hydrogels (Figure 5-a and Figure S5). Indeed, different degrees of stiffness and dissipation were only obtained by changing the permeability of the hydrogels in 4Cr composition. In a permeable hydrogel (coarse pore size, k~10^{-12} m^2), the influence of the flow-dependent source is minor, while it is a dominant dissipation source in

15

303 poorly permeable hydrogels (finer pores, $k \leq 10^{-14}$ m^2). We also observed that three porous

304 hydrogels (4Cr-Fine, 6Cr-Medium and 8Cr-Coarse) present similar ED to articular cartilage,[6,]

305 [46] under cyclic compression. The contribution of the dissipation sources in these hydrogels was

306 evaluated by measuring the ED ratio obtained from two different loading regimes as following.

307 The "standard regime" was a walking-like cyclic compression defined as 10% dynamic strain

308 at 1 Hz over 10% static strain. The "validation regime" represents another loading with lower

309 frequency (0.1 Hz) and larger dynamic strain (15%) over 5% static strain.

310 Being a function of the loading rate, fluid velocity and pressure are decreased in the

311 "validation regime" resulting in lower frictional drag dissipation. Accordingly, in the 4Cr-Fine

312 hydrogel with poor permeability, we observed a lower ED in the "validation regime" compared

313 to the "standard regime" as shown in Figure 5-b (ED ratio ~ 0.7). In parallel, by applying a

314 larger cyclic strain, an increased dynamic deformation is generated within the polymeric

315 network, which in turn leads to a higher flow-independent dissipation. Therefore, the 8Cr-

316 Coarse hydrogel with a dominant solid intrinsic dissipation showed higher ED level in the

317 "validation regime" compared to the "standard regime" (ED ratio ~ 1.2). In the intermediate

318 condition of the 6Cr-Medium hydrogel, no significant difference in the level of energy

319 dissipation was observed between the two applied loading regimes (ED ratio ~ 1). This

320 indicates that the influence of the decreased frequency and the increased dynamic strain

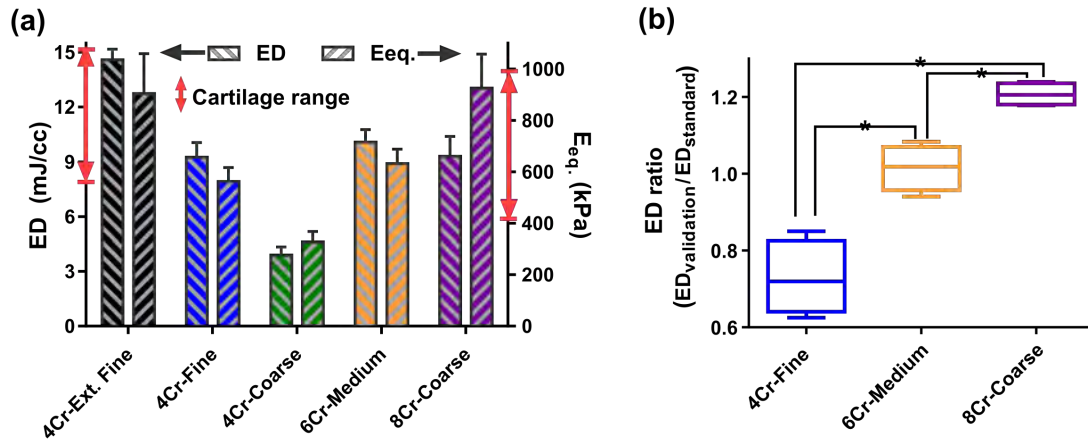321 compensate each other in the 6Cr-Medium hydrogel.

Figure 5. Mechanical properties of the porous pHEMA based hydrogels. (a) Energy dissipation level (ED, left axis) and equilibrium Young's modulus (Eeq, right axis) of the developed porous hydrogel along with the corresponding values for the cartilage shown by arrows (reported in references [1, 4, 6, 9]) in range of 10 to 20% strain. (b) Energy dissipation ratio of validation to standard loading regimes for porous hydrogels with similar dissipative capacity but different dissipation mechanisms (* significant difference with $p < 0.01$; n =4).

To validate the inverse correlation of the flow-dependent dissipation source to the permeability, we also increased the viscosity of the hydrogels fluid phase by using glycerol for the ED evaluation. It was observed that the ED level is further amplified in case of glycerol instead of water (Figure S6) for the 4Cr-Fine hydrogel compared to the 8Cr-Coarse hydrogel. A semi-inverse finite element model was used to evaluate the solid and fluid phases contribution to the viscoelastic behavior of the 8Cr-Coarse and the 4Cr-Fine hydrogels (Figure S7 & Table S3). It was shown that the load is partly carried by the solid phase in the 4Cr-Fine hydrogel with low permeability thanks to the support of the pressurized fluid (Figure S8). In contrast, contribution of developed fluid pressure was trivial to the load support capability of highly permeable 8Cr-Coarse hydrogels. We also observed that flow-independent viscoelasticity has a dominant role for 8Cr-Coarse hydrogels contrary to 4Cr-Fine hydrogels.

3.2.3 Analyzing fatigue performance and durability of porous hydrogels

For the porous hydrogels, the dissipation and stiffness values corresponding to the cartilage properties (Figure 5-a) are either obtained by a reduced permeability or an increased Cr ratio. Indeed, the consequent fatigue behavior could be significantly different, as presented in Figure 6, depending on the mechanism of dissipation. The shrinkage of the hysteresis loop area (Figure 6-a) was more significant in porous hydrogels with higher crosslinking ratio irrespective of their morphology. For instance, the 8Cr-Coarse hydrogel showed significantly weaker fatigue performance than the 4Cr-Coarse hydrogel with their normalized ED difference for cycles 10 and 100 being around 65% and 15%, respectively. Destructive dissipation mechanisms such as bonds rupture and/or chains fracture within the constrained network are likely contributing to this behavior as discussed earlier (in section 3.1).
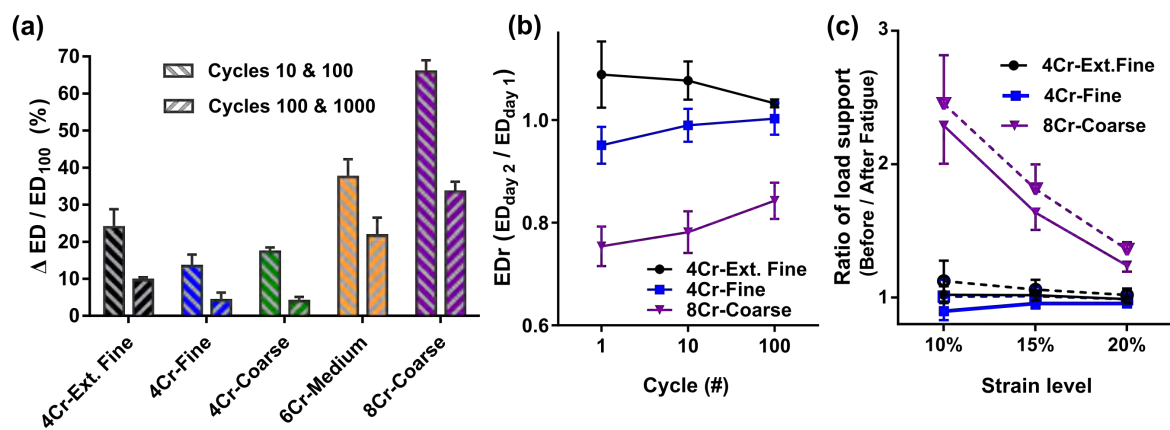

Figure 6. Fatigue performance of porous pHEMA based hydrogels. (a) The differential normalized value of the energy dissipation in standard loading regime for cycle 10 and 1000 with respect to cycle 100 as the reference cycle ($\frac{\Delta ED}{ED_{100}}$) where ΔED was calculated by subtraction of the latter cycle from the former cycle. (b) Recoverability of energy dissipation upon standard loading regime in two consecutive days while resting overnight in water after the first test. (c) Equilibrium load support ratio in sequential stress relaxation tests before and after fatigue loads (Dashed and solid lines show the data for one hour and one day recovery time, respectively).

18

360   To further scrutinize the role of irreversible processes in the evolution of hysteresis loops,

361   the ED recoverability (EDr) was compared for two identical cyclic loading experiments in two

362   consecutive days (see Figure S9). For this purpose, we selected hydrogels showing similar

363   stiffness and dissipative capacity with and without contribution of frictional drag force (e.g.,

364   4Cr-Ext. Fine and 4Cr-Fine versus 8Cr-Coarse). As shown in Figure 6-b, the recoverability of

365   the 8Cr-Coarse hydrogel was limited with an EDr value around 0.8. In contrast, a full recovery

366   (EDr ~1) was observed for hybridly crosslinked hydrogels with poor (4Cr-Ext. Fine) or low

367   (4Cr-Fine) permeability. This indicates that non-destructive processes arising from reversible

368   rearrangements of the network or fluid-solid interactions govern the hysteresis curve evolution

369   in 4Cr compositions. On the other hand, the permeable 8Cr-Coarse hydrogel with constrained

370   network loses its possibilities to dissipate energy over time, as its polymeric dissipation source

371   is self-sacrificial.

372   To evaluate hydrogels long-term durability, the ratio of the load support (R_{ls}) in equilibrium

373   state was measured before and after application of a walking-like cyclic loading as presented

374   in Figure 6-c. We obtained a preserved load support capability (R_{ls}~1) for 4Cr-Fine and 4Cr-

375   Ext. Fine porous hydrogels regardless of the permitted recovery time. Conversely, for 8Cr-

376   Coarse samples, a significant drop on the load support capability was observed despite a slight

377   recovery after a longer resting time (Figure 6-c). In particular, the ratio of the equilibrium load

378   support at 10% strain was around 2.2 in this case. The developed 4Cr hydrogels with coarse,

379   fine and extra fine pores had respectively similar morphology (Figure 4), dissipation level and

380   stiffness (Figure 5-a) to 8Cr-Coarse porous hydrogel. Accordingly, the fatigue resistance

381   performance is not a function of morphology, dissipation level, and stiffness of the viscoelastic

382   hydrogels but rather depends on the nature of the dissipation source. By a careful combination

383   of intrinsic network and fluidic frictional drag dissipations in a porous structure, fatigue

384   resistant hydrogels with relatively high stiffness, water fraction, and dissipative capacity could

385   therefore be developed.

386   **3.3   Mechanobiological performance of hydrogels with different dissipation sources**

387   Dynamic compression is the most widely employed loading regime in cartilage tissue

388   engineering and mechanobiology, where stimuli up to 20% compressive strain have promoted

389   chondrogenesis.[46-48] The dissipation of the cartilage tissue under cyclic compression originates

390   from matrix deformation and interstitial fluid flow,[6, 49] which are potential regulatory cues for

391   cells.[47] In this regard, a direct correlation was reported between the ED level of cell-seeded

392   scaffolds and chondrogenic expression following cyclic compression.[6] It was shown that

393   chondrogenic markers are at highest level for constructs with dissipation level similar to

394   healthy cartilage. However, it still remains to unravel the influence of dissipation sources on

395   chondrogenesis while mimicking the dissipative capacity of cartilage. For this purpose, we

396   examined the intracellular transcriptions of human chondro-progenitor cells,[35] embedded in the

397   4Cr-Fine and 8Cr-Coarse hydrogels following mechanical stimulation. These two groups of

398   hydrogels have a similar ED value (Figure 5-a) in the range of healthy cartilage, even though

399   their dissipative capacity originates from different sources. Having confirmed cells penetration

400   and viability up to 10 days in the developed dissipative hydrogels (Figure S10 and S11), we

401   evaluated cells differentiation by application of intermittent cyclic compressions. Collagen

402   type II (COL2A), Sex-determining region Y box 9 (SOX9) and Aggrecan (ACAN) genes were

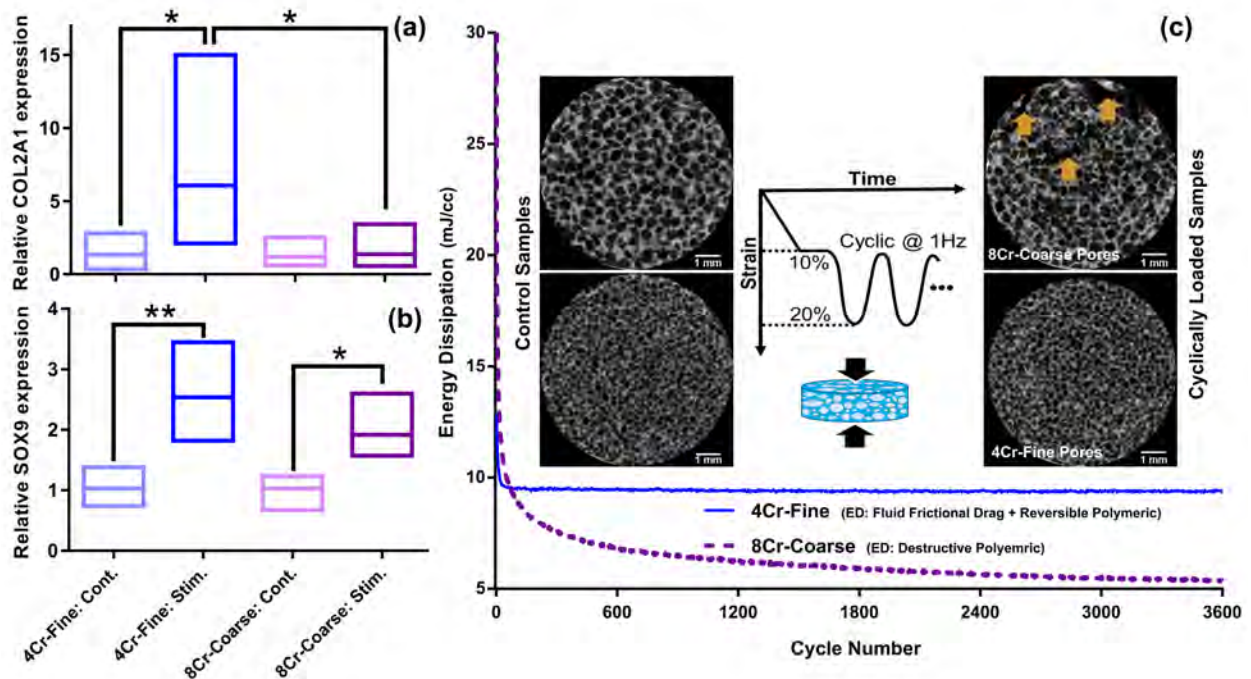403   evaluated for cells response as they are important indicators of chondrogenesis.[50]

Figure 7. Chondrogenic markers expression for human chondro-progenitor cells when seeded into two types of porous hydrogel presenting similar dissipative capacity (but originating from different sources) and water content to articular cartilage. (a-b) COL2A1 and SOX9 relative fold increase (depicted as mean value with minimum and maximum ranges) following cyclic compression in treatment (Stim.) group with respect to free swelling control (Cont.) group (* and ** mean significant difference with $p < 0.05$ and $p < 0.01$, respectively; n=4). (c) Evolution of the energy dissipation level following cyclic compression for the two types of dissipative hydrogel undergoing mechanical stimulation. Internal fissures (shown by arrows) appeared inside the 8Cr-Coarse hydrogel structure after repeated loading.

In general, the expression of chondrogenic markers was upregulated in the two groups of dissipative hydrogels by mechanical stimulation (Stim.) relative to corresponding free swelling control (Cont.) groups as shown in Figure 7 and Figure S12-b. Additionally, the enhanced mechanical performance obtained with a preserved hysteresis source could be further applied to mechanobiological function of hydrogels. Following the mechanical stimulation, a higher

419   relative fold increase was always obtained for chondrogenic markers in the 4Cr-Fine cells-

420   laden hydrogels compared to the 8Cr-Coarse constructs. In particular, a significant difference

421   was observed for COL2A1 gene expression (Figure 7-a) between the two hydrogel groups after

422   mechanical stimulation. Collagen type II fibrils form the structural network of the articular

423   cartilage and are the major constituent of the tissue solid matrix.

424   Mechanical hysteresis has been recently proposed to be an overarching mechanobiological

425   variable for mechanical cues in cartilage tissue.[6] Therefore, if the level of ED close to the

426   cartilage is the target recapitulating feature when applying a dynamic loading, hydrogels

427   possessing non-destructive mechanisms of dissipation should be designed. Given different

428   origins of energy dissipation in the two hydrogel groups, the seeded cells did not receive the

429   same physical cues despite applying a similar external stimulus on them. In the hydrogel group

430   deprived of reversible dissipation sources (8Cr-Coarse), the required physical cues cannot be

431   kept at an appropriate level via a constant loading regime. Conversely, for the hydrogel

432   presenting a preserved hysteresis loop (4Cr-Fine), the stimulation could be stabilized after a

433   few preconditioning cycles as illustrated in Figure 7-c. This latter hydrogel could even sustain

434   a 70% compressive strain without presenting a plastic deformation or defects unlike the 8Cr-

435   Coarse hydrogel (Figure S13).

436   The energy dissipation capability of the cartilage tissue originates from intrinsic matrix

437   viscoelasticity and interstitial fluid flow.[6,49] The influence of flow-dependent dissipation source

438   is trivial on hysteretic behavior of highly permeable 8Cr-Coarse hydrogels with inferior

439   mechanobiological performance. The effective contribution of the fluid frictional drag force to

440   the dissipative behavior of 4Cr-Fine hydrogels is likely a key factor for the enhanced response

441   of chondro-progenitor cells. Indeed, chondrocytes differentiation is favored by an artificial

442   niche, which mimics more similarly the cartilage extracellular environment (low permeability

443   and mobile matrix). An adequate frictional drag force in conjunction with a relatively high fluid

444   pressure and matrix deformation provide a chondro-inductive condition that probably stimulate

445   cells mechanosensitive elements (nucleus, ion channels, primary cilium, and cytoskeleton). [5,]

446   [47]

4   CONCLUSION

448   Fatigue resistant hydrogels presenting comparable stiffness, water content, and dissipation

449   level to cartilage were developed by controlling specific sources of dissipation. The preserved

450   hysteresis and load support capability were obtained by a combination of reversible polymeric

451   and fluid frictional drag dissipations. The hydrogel network was synthesized based on hybrid

452   crosslinking approach to control flow-independent mechanism of dissipation. In parallel, a

453   porous morphology with a controlled permeability was engineered to enhance flow-dependent

454   source of dissipation in hydrogels with relatively high water fraction. It was shown that

455   hydrogels with comparable morphology, stiffness, or dissipation level respond to fatigue

456   loadings in a significant different way, depending on their sources of dissipation. Moreover,

457   we demonstrated that the mechanism of dissipation could play an important role in the

458   chondrogenic differentiation of cells following cyclic compression. While fundamentally

459   different physical processes can generate similar dissipation level under loading,

460   chondrogenesis is favored by a preserved dissipation with an active flow-dependent source.

461   These findings indicate that not only the fluid frictional drag dissipation protects biomaterials

462   under fatigue loading but also is a promoting mechanobiological regulator for chondrocytes.

463   Collectively, major opportunities towards development of load-bearing biomaterials could be

464   derived from control of dissipation sources. The proposed strategy in development of load-

465   bearing hydrogels, which combines fluidic with polymeric dissipation sources, can be widely

466   used in functional tissue engineering.

467   **ASSOCIATED CONTENT**

468   **Supporting information:**

469   Conventional hydrogels load support capability before and after fatigue loading, tensile

470   properties of conventional hydrogels, effect of initiator type on porous hydrogels mechanical

471   properties, separation of solid and fluid phases contribution to load support, effect of the fluidic

472   phase viscosity on energy dissipation, and cells distribution and viability in porous hydrogels

473   are presented in supporting information. In addition, a complete description of the methods

474   used for experimental and computational characterization of hydrogels can be found in

475   supporting information.

476 **AUTHOR INFORMATION**

477 **Corresponding author**

478 Dominique Pioletti. *Email:dominique.pioletti@epfl.ch

479 EPFL/STI/IBI/LBO, Station 9

480 1015 Lausanne-Switzerland

481 **Author Contributions:**

482 NN designed and developed the hydrogels and performed the experimental and biological tests.

483 NN, PK and DPP contributed to the analysis of the results. DPP conceptualized and supervised

484 the project. NN wrote the manuscript and prepared the figures. PK designed the schematic

485 figures. DPP and PK reviewed the manuscript.

489 **ACKNOWLEDGMENT**

5   REFERENCES

494   1.   Moutos, F. T.; Freed, L. E.; Guilak, F., A Biomimetic Three-Dimensional Woven
495   Composite Scaffold for Functional Tissue Engineering of Cartilage. *Nat. Mater.* **2007,** *6* (2),
496   162.
497   2.   Liao, I. C.; Moutos, F. T.; Estes, B. T.; Zhao, X.; Guilak, F., Composite Three-
498   Dimensional Woven Scaffolds with Interpenetrating Network Hydrogels to Create Functional
499   Synthetic Articular Cartilage. *Adv. Funct. Mater.* **2013,** *23* (47), 5833-5839.
500   3.   Hong, S.; Sycks, D.; Chan, H. F.; Lin, S.; Lopez, G. P.; Guilak, F.; Leong, K. W.; Zhao,
501   X., 3d Printing of Highly Stretchable and Tough Hydrogels into Complex, Cellularized
502   Structures. *Adv. Mater.* **2015,** *27* (27), 4035-4040.
503   4.   Mow, V. C.; Ratcliffe, A.; Poole, A. R., Cartilage and Diarthrodial Joints as Paradigms
504   for Hierarchical Materials and Structures. *Biomaterials* **1992,** *13* (2), 67-97.
505   5.   Mow, V. C.; Wang, C. C.; Hung, C. T., The Extracellular Matrix, Interstitial Fluid and
506   Ions as a Mechanical Signal Transducer in Articular Cartilage. *Osteoarthr. Cartil.* **1999,** *7* (1),
507   41-58.
508   6.   Abdel-Sayed, P.; Darwiche, S. E.; Kettenberger, U.; Pioletti, D. P., The Role of Energy
509   Dissipation of Polymeric Scaffolds in the Mechanobiological Modulation of Chondrogenic
510   Expression. *Biomaterials* **2014,** *35* (6), 1890-1897.
511   7.   Lee, H.-p.; Gu, L.; Mooney, D. J.; Levenston, M. E.; Chaudhuri, O., Mechanical
512   Confinement Regulates Cartilage Matrix Formation by Chondrocytes. *Nat. Mater.* **2017,** *16*
513   (12), 1243.
514   8.   Chaudhuri, O.; Gu, L.; Klumpers, D.; Darnell, M.; Bencherif, S. A.; Weaver, J. C.;
515   Huebsch, N.; Lee, H.-p.; Lippens, E.; Duda, G. N., Hydrogels with Tunable Stress Relaxation
516   Regulate Stem Cell Fate and Activity. *Nat. Mater.* **2016,** *15* (3), 326-334.
517   9.   Abdel-Sayed, P.; Vogel, A.; Nassajian Moghadam, M.; Pioletti, D., Cartilage Self-
518   Heating Contributes to Chondrogenic Expression. *European Cells and Materials* **2013,** *26*
519   (EPFL-ARTICLE-188814), 171-178.
520   10.   Zhao, X., Multi-Scale Multi-Mechanism Design of Tough Hydrogels: Building
521   Dissipation into Stretchy Networks. *Soft Matter* **2014,** *10* (5), 672-687.
522   11.   Long, R.; Hui, C.-Y., Fracture Toughness of Hydrogels: Measurement and
523   Interpretation. *Soft Matter* **2016,** *12* (39), 8069-8086.
524   12.   Gong, J. P.; Katsuyama, Y.; Kurokawa, T.; Osada, Y., Double-Network Hydrogels with
525   Extremely High Mechanical Strength. *Adv. Mater.* **2003,** *15* (14), 1155-1158.
526   13.   Sun, J.-Y.; Zhao, X.; Illeperuma, W. R.; Chaudhuri, O.; Oh, K. H.; Mooney, D. J.;
527   Vlassak, J. J.; Suo, Z., Highly Stretchable and Tough Hydrogels. *Nature* **2012,** *489* (7414),
528   133.
529   14.   Abdurrahmanoglu, S.; Can, V.; Okay, O., Design of High-Toughness Polyacrylamide
530   Hydrogels by Hydrophobic Modification. *Polymer* **2009,** *50* (23), 5449-5455.
531   15.   Henderson, K. J.; Zhou, T. C.; Otim, K. J.; Shull, K. R., Ionically Cross-Linked
532   Triblock Copolymer Hydrogels with High Strength. *Macromolecules* **2010,** *43* (14), 6193-
533   6201.

534 16.   Sun, T. L.; Kurokawa, T.; Kuroda, S.; Ihsan, A. B.; Akasaki, T.; Sato, K.; Haque, M.
535 A.; Nakajima, T.; Gong, J. P., Physical Hydrogels Composed of Polyampholytes Demonstrate
536 High Toughness and Viscoelasticity. *Nat. Mater.* **2013,** *12* (10), 932.
537 17.   Li, J.; Suo, Z.; Vlassak, J. J., Stiff, Strong, and Tough Hydrogels with Good Chemical
538 Stability. *Journal of Materials Chemistry B* **2014,** *2* (39), 6708-6713.
539 18.   Karami, P.; Wyss, C. l. S.; Khoushabi, A.; Schmocker, A.; Broome, M.; Moser, C.;
540 Bourban, P.-E.; Pioletti, D. P., Composite Double-Network Hydrogels to Improve Adhesion
541 on Biological Surfaces. *ACS Appl. Mater. Interfaces* **2018,** *10* (45), 38692-38699.
542 19.   Chen, Q.; Zhu, L.; Chen, H.; Yan, H.; Huang, L.; Yang, J.; Zheng, J., A Novel Design
543 Strategy for Fully Physically Linked Double Network Hydrogels with Tough, Fatigue
544 Resistant, and Self-Healing Properties. *Adv. Funct. Mater.* **2015,** *25* (10), 1598-1607.
545 20.   Bai, R.; Yang, Q.; Tang, J.; Morelle, X. P.; Vlassak, J.; Suo, Z., Fatigue Fracture of
546 Tough Hydrogels. *Extreme Mechanics Letters* **2017,** *15*, 91-96.
547 21.   Yuan, N.; Xu, L.; Wang, H.; Fu, Y.; Zhang, Z.; Liu, L.; Wang, C.; Zhao, J.; Rong, J.,
548 Dual Physically Cross-Linked Double Network Hydrogels with High Mechanical Strength,
549 Fatigue Resistance, Notch-Insensitivity, and Self-Healing Properties. *ACS Appl. Mater.*
550 *Interfaces* **2016,** *8* (49), 34034-34044.
551 22.   Lin, S.; Liu, X.; Liu, J.; Yuk, H.; Loh, H.-C.; Parada, G. A.; Settens, C.; Song, J.; Masic,
552 A.; McKinley, G. H., Anti-Fatigue-Fracture Hydrogels. *Science advances* **2019,** *5* (1),
553 eaau8528.
554 23.   Li, J.; Illeperuma, W. R.; Suo, Z.; Vlassak, J. J., Hybrid Hydrogels with Extremely High
555 Stiffness and Toughness. *ACS Macro Letters* **2014,** *3* (6), 520-523.
556 24.   Luo, F.; Sun, T. L.; Nakajima, T.; Kurokawa, T.; Zhao, Y.; Sato, K.; Ihsan, A. B.; Li,
557 X.; Guo, H.; Gong, J. P., Oppositely Charged Polyelectrolytes Form Tough, Self-Healing, and
558 Rebuildable Hydrogels. *Adv. Mater.* **2015,** *27* (17), 2722-2727.
559 25.   Zhang, Y.; Gao, H.; Wang, H.; Xu, Z.; Chen, X.; Liu, B.; Shi, Y.; Lu, Y.; Wen, L.; Li,
560 Y., Radiopaque Highly Stiff and Tough Shape Memory Hydrogel Microcoils for Permanent
561 Embolization of Arteries. *Adv. Funct. Mater.* **2018,** *28* (9), 1705962.
562 26.   Gong, J. P., Materials Both Tough and Soft. *Science* **2014,** *344* (6180), 161-162.
563 27.   Nasrollahzadeh, N.; Pioletti, D. P., Experimental Method to Characterize the Strain
564 Dependent Permeability of Tissue Engineering Scaffolds. *J. Biomech.* **2016,** *49* (15), 3749-
565 3752.
566 28.   Mow, V. C.; Kuei, S.; Lai, W. M.; Armstrong, C. G., Biphasic Creep and Stress
567 Relaxation of Articular Cartilage in Compression: Theory and Experiments. *J. Biomech. Eng.*
568 **1980,** *102* (1), 73-84.
569 29.   Peppas, N. A.; Moynihan, H. J.; Lucht, L. M., The Structure of Highly Crosslinked Poly
570 (2-Hydroxyethyl Methacrylate) Hydrogels. *J. Biomed. Mater. Res. A* **1985,** *19* (4), 397-411.
571 30.   Khoushabi, A.; Schmocker, A.; Pioletti, D.; Moser, C.; Schizas, C.; Månson, J.-A.;
572 Bourban, P.-E., Photo-Polymerization, Swelling and Mechanical Properties of Cellulose Fibre
573 Reinforced Poly (Ethylene Glycol) Hydrogels. *Composites Sci. Technol.* **2015,** *119*, 93-99.
574 31.   Suh, J.-K.; DiSilvestro, M., Biphasic Poroviscoelastic Behavior of Hydrated Biological
575 Soft Tissue. *Journal of Applied Mechanics* **1999,** *66* (2), 528-535.
576 32.   Simon, B. R., Multiphase Poroelastic Finite Element Models for Soft Tissue Structures.
577 *Applied Mechanics Reviews* **1992,** *45* (6), 191-218.
578 33.   Roylance, D., *Mechanics of Materials*. John Wiley & Sons: New York, 1996.
579 34.   Allahverdizadeh, A.; Mahjoob, M. J.; Nasrollahzadeh, N.; Eshraghi, I., Optimal
580 Parameters Estimation and Vibration Control of a Viscoelastic Adaptive Sandwich Beam
581 Incorporating an Electrorheological Fluid Layer. *J. Vibrat. Control* **2014,** *20* (12), 1855-1868.

582   35.   Darwiche, S.; Scaletta, C.; Raffoul, W.; Pioletti, D. P.; Applegate, L. A., Epiphyseal
583   Chondroprogenitors Provide a Stable Cell Source for Cartilage Cell Therapy. *Cell Medicine*
584   **2012,** *4* (1), 23-32.
585   36.   Nasrollahzadeh, N.; Applegate, L. A.; Pioletti, D. P., Development of an Effective Cell
586   Seeding Technique: Simulation, Implementation, and Analysis of Contributing Factors. *Tissue*
587   *Eng.,Part C* **2017,** *23* (8), 485-496.
588   37.   Moghadam, M. N.; Pioletti, D. P., Improving Hydrogels' Toughness by Increasing the
589   Dissipative Properties of Their Network. *J. Mech. Behav. Biomed. Mater.* **2015,** *41*, 161-167.
590   38.   Annabi, N.; Nichol, J. W.; Zhong, X.; Ji, C.; Koshy, S.; Khademhosseini, A.; Dehghani,
591   F., Controlling the Porosity and Microarchitecture of Hydrogels for Tissue Engineering. *Tissue*
592   *Eng.,Part B* **2010,** *16* (4), 371-383.
593   39.   Refojo, M. F., Hydrophobic Interaction in Poly (2-Hydroxyethyl Methacrylate)
594   Homogeneous Hydrogel. *J. Polym. Sci., Part A: Polym. Chem.* **1967,** *5* (12), 3103-3113.
595   40.   Karpushkin, E.; Dušková-Smrčková, M.; Šlouf, M.; Dušek, K., Rheology and Porosity
596   Control of Poly (2-Hydroxyethyl Methacrylate) Hydrogels. *Polymer* **2013,** *54* (2), 661-672.
597   41.   Ratner, B. D.; Miller, I. F., Interaction of Urea with Poly (2-Hydroxyethyl
598   Methacrylate) Hydrogels. *Journal of Polymer Science Part A-1: Polymer Chemistry* **1972,** *10*
599   (8), 2425-2445.
600   42.   Morita, S., Hydrogen-Bonds Structure in Poly (2-Hydroxyethyl Methacrylate) Studied
601   by Temperature-Dependent Infrared Spectroscopy. *Front. Chem.* **2014,** *2*, 10.
602   43.   Choi, S.; Jhon, M. S.; Andrade, J. D., Nature of Water in Synthetic Hydrogels: Iii.
603   Dilatometry, Specific Conductivity, and Dielectric Relaxation of Poly (2, 3-Dihydroxypropyl
604   Methacrylate). *Journal of Colloid and Interface Science* **1977,** *61* (1), 1-8.
605   44.   Granke, M.; Does, M. D.; Nyman, J. S., The Role of Water Compartments in the
606   Material Properties of Cortical Bone. *Calcif. Tissue Int.* **2015,** *97* (3), 292-307.
607   45.   Lai, W.; Mow, V. C.; Roth, V., Effects of Nonlinear Strain-Dependent Permeability
608   and Rate of Compression on the Stress Behavior of Articular Cartilage. *J. Biomech. Eng.* **1981,**
609   *103* (2), 61-66.
610   46.   Salinas, E. Y.; Hu, J. C.; Athanasiou, K., A Guide for Using Mechanical Stimulation to
611   Enhance Tissue-Engineered Articular Cartilage Properties. *Tissue Eng.,Part B* **2018**.
612   47.   O'Conor, C. J.; Case, N.; Guilak, F., Mechanical Regulation of Chondrogenesis. *Stem*
613   *Cell Res Ther* **2013,** *4* (4), 61.
614   48.   Finlay, S.; Seedhom, B. B.; Carey, D. O.; Bulpitt, A. J.; Treanor, D. E.; Kirkham, J., In
615   Vitro Engineering of High Modulus Cartilage-Like Constructs. *Tissue Eng.,Part C* **2016,** *22*
616   (4), 382-397.
617   49.   Mak, A., The Apparent Viscoelastic Behavior of Articular Cartilage—the
618   Contributions from the Intrinsic Matrix Viscoelasticity and Interstitial Fluid Flows. *J. Biomech.*
619   *Eng.* **1986,** *108* (2), 123-130.
620   50.   Huang, A. H.; Farrell, M. J.; Mauck, R. L., Mechanics and Mechanobiology of
621   Mesenchymal Stem Cell-Based Engineered Cartilage. *J. Biomech.* **2010,** *43* (1), 128-136.

622

623

624

6 <mark>**Table of Contents Graphic**</mark>

626
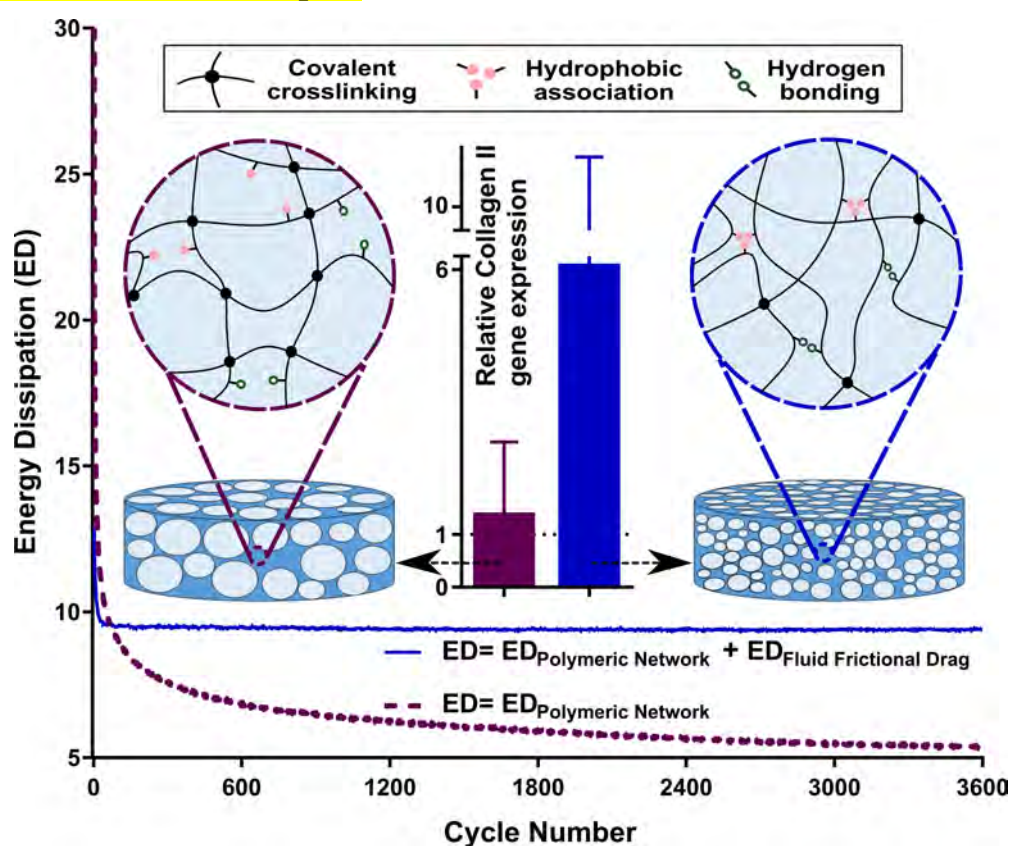
Supporting information

Control of dissipation sources: A central aspect for enhancing the mechanical and mechanobiological performances of hydrogels

Naser Nasrollahzadeh, Peyman Karami, Dominique P. Pioletti*.

Laboratory of Biomechanical Orthopedics, Institute of Bioengineering, EPFL, 1015 Lausanne Switzerland.

Corresponding Author's email address:dominique.pioletti@epfl.ch

Conventional hydrogels load support capability before and after fatigue loading

Three sequential unconfined compressions and hold steps were applied on the hydrogels to evaluate their mechanical behavior before and after the fatigue load as illustrated in Figure S1.
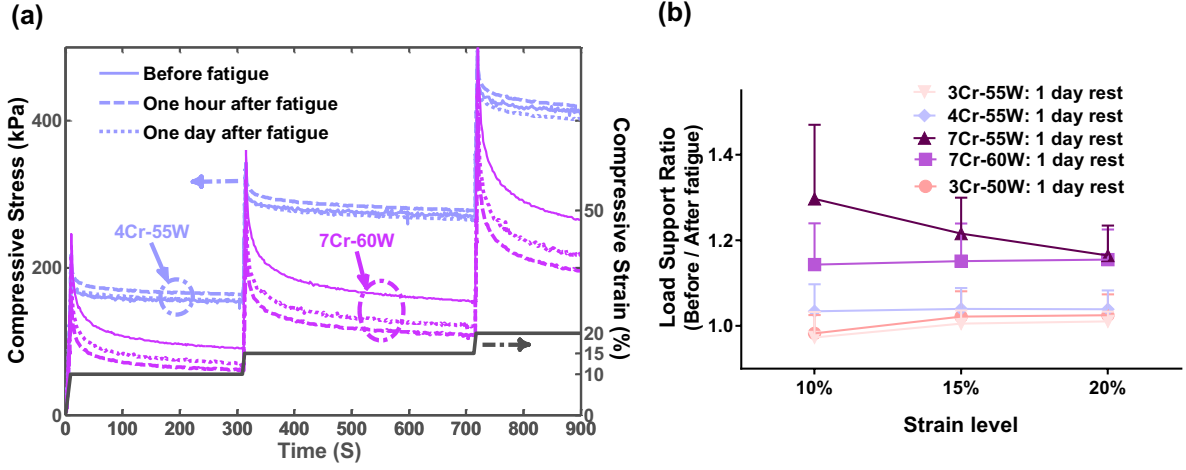
Figure S1. Conventional pHEMA based hydrogels load support capability. (a) Time dependent load support of 7Cr-60W (purple) and 4Cr-55W (blue) in sequential stress relaxation (ramp and hold strain) tests before and after fatigue load of 3600 cycles (10% static strain + 15% dynamic strain at 1 Hz). (b) Equilibrium load support ratio (n=3 per group).

Structural characteristics of conventional hydrogels

By evaluating the polymer volume fraction immediately after polymerization (as prepared) in relaxed state (v_{ap}) and after swelling in water (v_{sw}), the average molecular weight between crosslinks (M_C) for hydrogel prepared in the presence of water can be determined using modified Flory–Rehner theory [1] by (S1):

$$\frac{1}{M_c} = \frac{2}{M_n} - \frac{\left(\frac{\bar{v}}{V_1}\right)\left[\ln(1 - v_{sw}) + v_{sw} + \chi v_{sw}^2\right]}{v_{ap}\left[\left(\frac{v_{sw}}{v_{ap}}\right)^{1/3} - \left(\frac{v_{sw}}{2v_{ap}}\right)\right]} \tag{S1}$$

where M_n is the average chains length (considered here equal to 400 unit monomer of HEMA, $M_n \approx 54000$ g/mol) , $\bar{v}$ is the specific volume of polymer, V_1 is the molar volume of water (18.03 ml), and χ is the thermodynamics interaction parameter determined as:

$$\chi = 0.320 + 0.904 v_{sw} \tag{S2}$$

The mesh size can then be calculated using equation (S3):

$$\xi = v_{sw}^{-1/3} \times \frac{2M_c C_n}{M_r} \times l \tag{S3}$$

Where ξ is the mesh size, M_r is the molecular weight of HEMA unit monomer (134.12 g/mol), C_n is the Flory characteristic ratio (6.9 for HEMA) and l the length of the bond along the polymer backbone (1.54 Å).

Table S1. Conventional pHEMA based hydrogels characteristics[a]

Hydrogel	Q_v	υ_{sw}	v_{ap}	χ	M_c (g/mol)	ξ (nm)	Appearance[b]
3%Cr-50%W	0.92 ±0.07	0.55 ±0.01	0.50 ±0.05	0.82	3842 ±861	3.72 ±0.45	
7%Cr-60%W	1.10 ±0.02	0.37 ±0.02	0.41 ±0.02	0.65	1931 ±354	3.00 ±0.23	
3%Cr-55%W	0.88 ±0.01	0.52 ±0.01	0.46 ±0.01	0.79	9210 ±948	5.90 ±0.32	
4%Cr-55%W	1.00 ±0.01	0.50 ±0.01	0.50 ±0.01	0.77	13120 ±176	7.13 ±0.07	
7%Cr-55%W	1.13 ±0.06	0.39 ±0.01	0.44 ±0.01	0.67	2492 ±151	3.36 ±0.08	

a: All average molecular weights (M_c) were calculated by assuming M_n=54000 g/mol.
b: The square has 10 mm length.

Tensile properties of conventional hydrogels

We prepared dumbbell shape hydrogels and extracted the tensile properties of the samples as shown in Figure S2. The tensile tests generally confirmed the results of compressive loading regime in different groups of hydrogels (e.g., similar trends for modulus, dissipative capacity and fatigue performance). In line with compressive results, the 4Cr-55W hydrogel showed fatigue resistance and full recoverability while presenting higher dissipative capacity and stiffness than 3Cr-55W and 3Cr-50W hydrogels. The 7Cr-55W hydrogel again showed highest stiffness but poor fatigue performance as it could not sustain 20 cycles of tensile loading without showing crack. The failure strain of 7Cr-60W hydrogels was very limited (~10%) and could not sustain any cyclic loading in tensile mode.
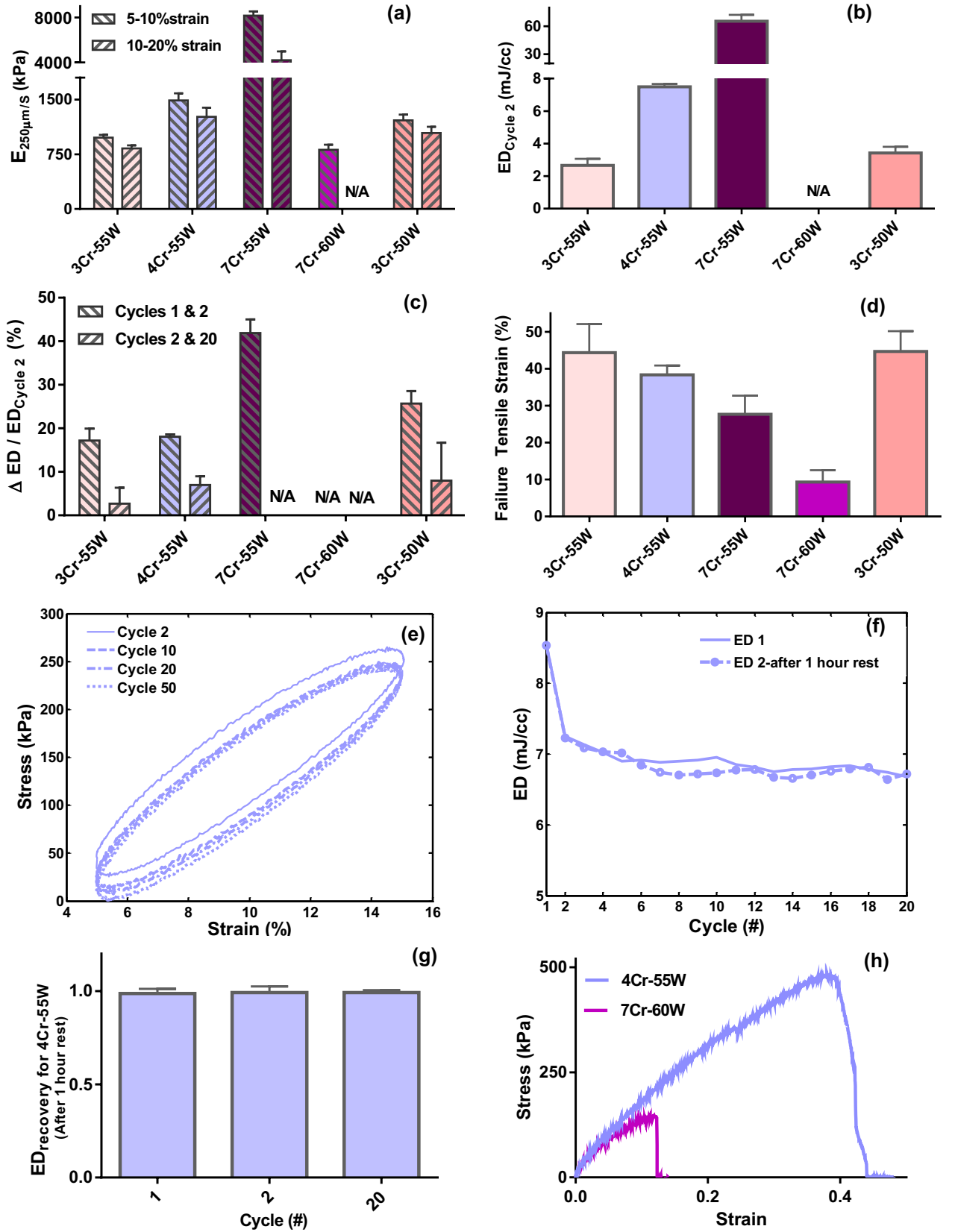
Figure S2. Tensile properties of pHEMA based hydrogels (N/A: not applicable). (a) Young modulus in different strain ranges at 250 μm/s loading rate. (b) Energy dissipation per unit volume by application of 5% pre-strain and 10% cyclic strain. (c) The differential value of the energy dissipation (ΔED) during repeated loadings at 0.2 Hz for cycle 1 and 20 normalized with value of cycle 2 as reference (ΔED/ED_{ref}) where ΔED was calculated by subtraction of the latter cycle from the former cycle. (d) Failure strain of different hydrogels following streching

at 250 µm/s loading rate. (e) Hysteresis loop evolution for 4Cr-55W hydrogel up to 50 cycles at 0.2 Hz. (f) Typical hysteresis loop area variation for 4Cr-55W hydrogel during cyclic loading. (g) Recoverability of energy dissipation for 4Cr-55W hydrogel durring two consecutive tests with one hour recovery time in water between the tests. (h) Typical stress-strain curves durring tension tests of 4Cr-55W and 7Cr-60W hydrogels.

Effect of initiator type on porous hydrogels mechanical properties

By testing different initiator for the polymerization process, we realized that the mechanical properties of porous hydrogels could be improved with different initiator agents as shown in Figure S3. Since porous hydrogels do not initially contain high water amount, contrary to conventional hydrogels, we could employ heat polymerization without significant loss of water during the fabrication process instead of UV polymerization by DPAP (57 mg/ml of ethanol). We therefore utilized 40 µl ammonium persulfate (AP, 100 mg/ml of water) and 40 µl sodium metabisulfite (SM, 100 mg/mL of water) redox initiator solution (AP-SM, polymerization time: 2 hours) instead of 40 µl photo initiator solution (DPAP, polymerization time: 15 minutes) for 1 ml HEMA and compared the corresponding mechanical properties of porous 4Cr-Fine hydrogel.
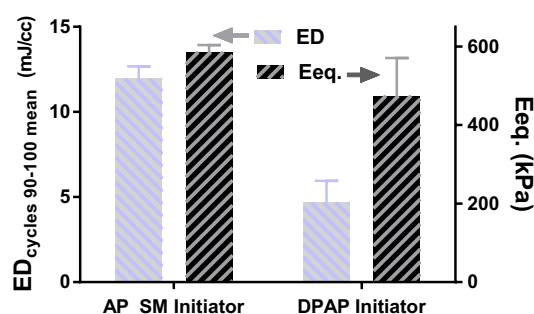
Figure S3. Equilibrium Young modulus (Eeq.) in range of 10 to 20% compressive strain and the level of energy dissipation (ED) by applying 10% dynamic strain over 10% static strain at 1 Hz on 4Cr-Fine porous hydrogels polymerized with different initiators.

Porous hydrogels structural characteristics

The salt particles were manually sieved in 7 different sizes from 100 to 500 µm. Then, different salt groups were combined with predefined ratio (Table S2) to modulate permeability (k) of the porous hydrogels. The salts were firstly put inside the mold and we then added precursor to the mold containing salts while maintaining salts to polymer ratio (2/1 Volumetric). In our study, we have a similar polymeric volume fraction (~30%) for all porous hydrogels while the crosslinker concentration is different varying from 4 to 8 percent molar ratio with respect to HEMA content. It is not possible to add a high volume of water in the precursor of porous hydrogels as it could dissolve the salts particles before polymerization. After polymerization of the precursor and during salt-leaching step in water, the polymer fraction of the porous

structure absorb water and swell while the salt particles are replaced by water. At the end of this process, porous hydrogels gain an equilibrium water content of around 70%.

Table S2. Characteristics of porous pHEMA hydrogels prepared with heat polymerization.

Hydrogel Type	Salt Size (µm)	EWC (%)	k at 0% strain (m^2)	k at 20% strain (m^2)
8%Cr-Coarse Pores	300-350: 60% 400-500: 40%	67±3	1.76E-12 ±5.04E-13	1.22E-12 ±3.72E-13
6%Cr-Medium Pores	250-300: 55% 300-350: 45%	68±2	5.10E-13 ±2.65E-13	2.08E-13 ±4.22E-14
4%Cr-Fine Pores	200-250: 80% 150-200: 20%	68±2	1.09E-14 ±1.55E-14	2.35E-15 ±3.07E-15
4%Cr-Coarse Pores	300-350: 60% 400-500: 40%	69±2	O(E-12)[a]	O(E-12)[a]
4%Cr-Extra Fine	100-150: 100%	69±1	< O(E-16)[b]	< O(E-16)[b]

a: we estimate the permeability (k) of the 4Cr-Coarse hydrogels to be in the same order of the 8Cr-Coarse hydrogels considering their similar pores distribution (Figure 4), EWC and morphology (the samples stiffness was not adequate for a reliable measurement based on a radial sealing (press fit) method [2]).

b: it was difficult to precisely measure the permeability of the porous 4Cr-Ext. Fine hydrogels due to very slow flow rate and long required time for passing a detectable amount of water without evaporation. However, we can safely estimate based on our previous work [2] that the permeability of this group is lower than 10^{-16} m^2.

The micro CT scans of porous hydrogels confirmed that the pores distribution is quite homogenous within different groups. As shown in Figure S4 fabricated samples with different salt groups (coarse, fine and extra fine) have similar pores distribution in all directions with a random pores orientation while their pore sizes are different.
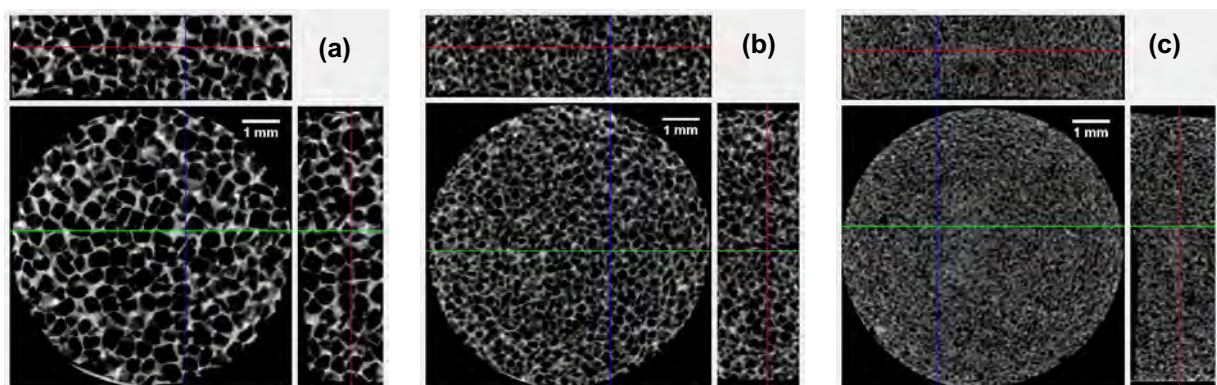

Figure S4. Micro-CT scans of freeze-dried scaffolds from different views. (a) Coarse pores. (b) Fine pores. (c) Extra Fine pores.

Porous hydrogels mechanical characterization

All samples were preconditioned firstly to consider the effect of cell seeding loading step on the mechanical properties of porous hydrogels. For this purpose, samples were submitted to a

predefined loading regime (30-35% compressive strain for 5 times) according to the compression-induced suction (CRIS) seeding method [3] and then rested inside water overnight before all characterization tests. Sequential stress relaxation tests (Figure S5) were carried out as described for the conventional hydrogels. However, to measure the energy dissipation, we applied 10% cyclic compression for porous hydrogels over 10% pre-strain at 1 Hz. A custom-written MATLAB script (The MathWorks, Natick, MA, USA) was used to extract the enclosed hysteresis area from the load-displacement graphs (Figure S5).
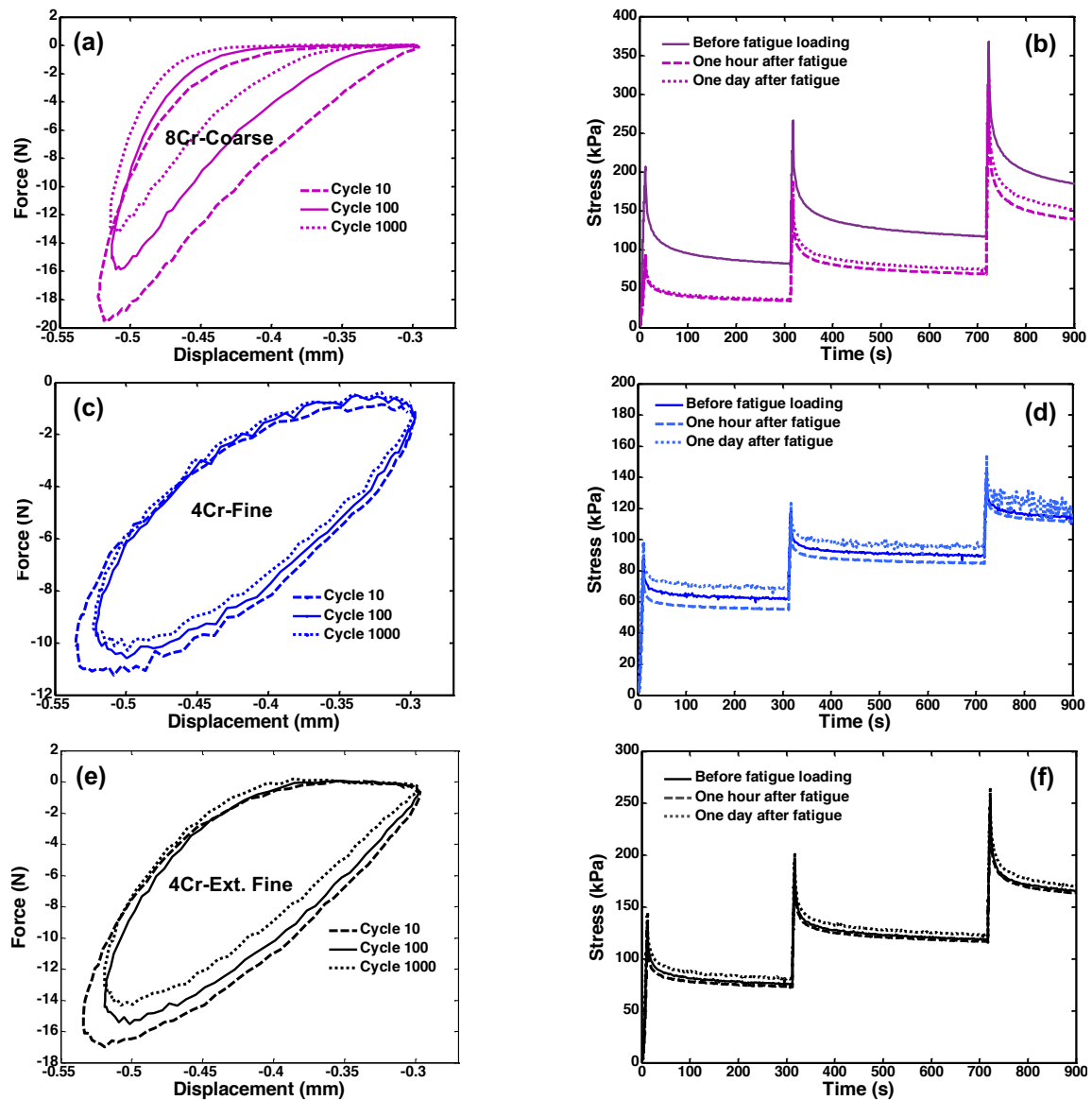
Figure S5. Mechanical behavior of porous pHEMA based hydrogels prepared with heat polymerization. (a,c & e) Representative hysteresis loop evolution for 8Cr-Coarse (purple), 4Cr-Fine (blue) and 4Cr-Extra Fine (black) during cyclic loading. (b,d & f) Representative time dependent load support of 8Cr-Coarse (purple), 4Cr-Fine (blue) and 4Cr-Extra Fine (black) in sequential stress relaxation (ramp and hold strain) tests before and after fatigue load of 3600 cycles (10% static strain+10% dynamic strain at 1Hz).

Effect of the fluidic phase viscosity on energy dissipation

To validate the inverse correlation of the flow-dependent dissipation source to the permeability, we increased the viscosity of the fluidic phase of the hydrogel by using glycerol instead of water for the ED evaluation. As shown in Figure S6, the ED level was further amplified with glycerol compared to water for the 4Cr-Fine hydrogel having a lower permeability ($k \sim 10^{-14}$) than 8Cr-Coarse hydrogel ($k \sim 10^{-12}$). This increase is much more significant in early cycles when the pores still contain considerable amount of glycerol. Due to lower permeability of 4Cr-Fine hydrogels, the glycerol with higher viscosity cannot refill the pores during unloading time following an applied compression, which enforces fluid seepage. Therefore, the ED is being decreased during cyclic loading.
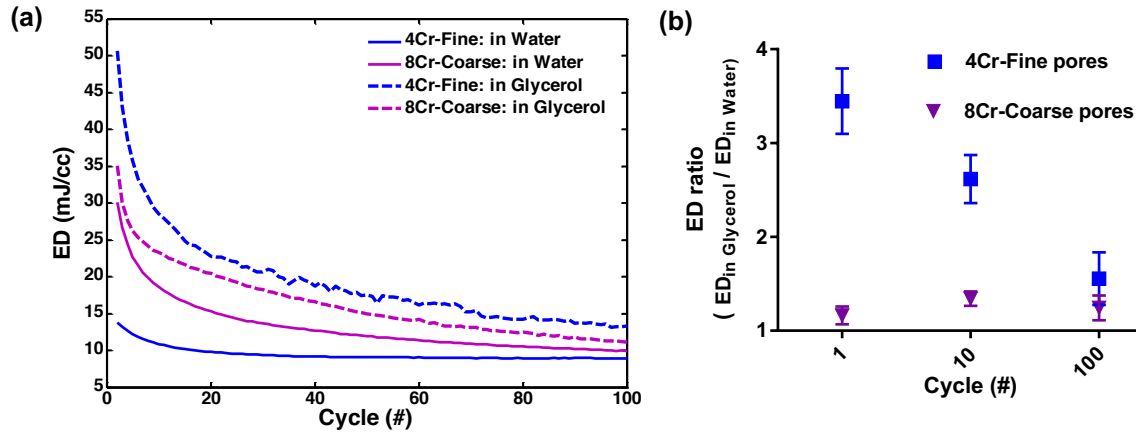
Figure S6. Effect of the fluidic phase viscosity on dissipative behavior of different porous hydrogels. (a) Typical trends of ED level with different fluid viscosities over the applied loading cycles for 4Cr-Fine and 8Cr-Coarse hydrogels. (b) Comparison of ED ratio in cycles 1, 10 and 100 in two groups (mean and SD, n=4).

Separation of solid and fluid phases contribution to load support

We combined experimental characterization and computational optimization to separate the flow-dependent and the flow-independent part of the load support by developing a poro-viscoelastic (PVE) model [4-5]. In the model, the 2D axisymmetric cross section of cylindrical samples having 2.5 mm thickness and 4 mm radius was divided to finite elements (Figure S7-a). Different material properties for a poro-viscoelastic model are required including equilibrium Young modulus (Eeq), strain dependent permeability (k(ε)), porosity (φ), Poisson ratio (ν) and relaxation function (G(t)) which is usually approximated by a Prony Series (e.g., G(t)= G + $\sum$G$_i$ e$^{-t/\tau i}$). Having measured Eeq, k(ε), ν and φ by relevant experiments, relaxation moduli (G$_i$) and times (τ_i) were estimated by an iterative process using particle swarm optimization (PSO) [6] to obtain the same trend of stress relaxation for the model and the experimental data (Figure S7-b). The objective function (OF) for PSO was defined according

to equation S4, in which we considered peak and equilibrium stresses (σ) along with stress decay rates ($\frac{d\sigma}{dt}$) at critical time points of relaxation curve.

$$OF = \sum w_i \ (\sigma^{exp} - \sigma^m)^2 + \sum u_i \ (\frac{d\sigma^{exp}}{dt} - \frac{d\sigma^m}{dt})^2 \tag{S4}$$

In equation S4, σ^{exp} is the nominal stress obtained from our experiment ($\sigma^{exp}(t) = \frac{F(t)}{A_{initial}}$), σ^m is the total stress obtained from the PVE model which consists of solid phase stress and fluid pressure ($\sigma^m = \sigma_{soild} + p_{fluid}$). Additionally, w_i and u_i are weighting coefficients and assigned based on the importance of the employed time points [7].
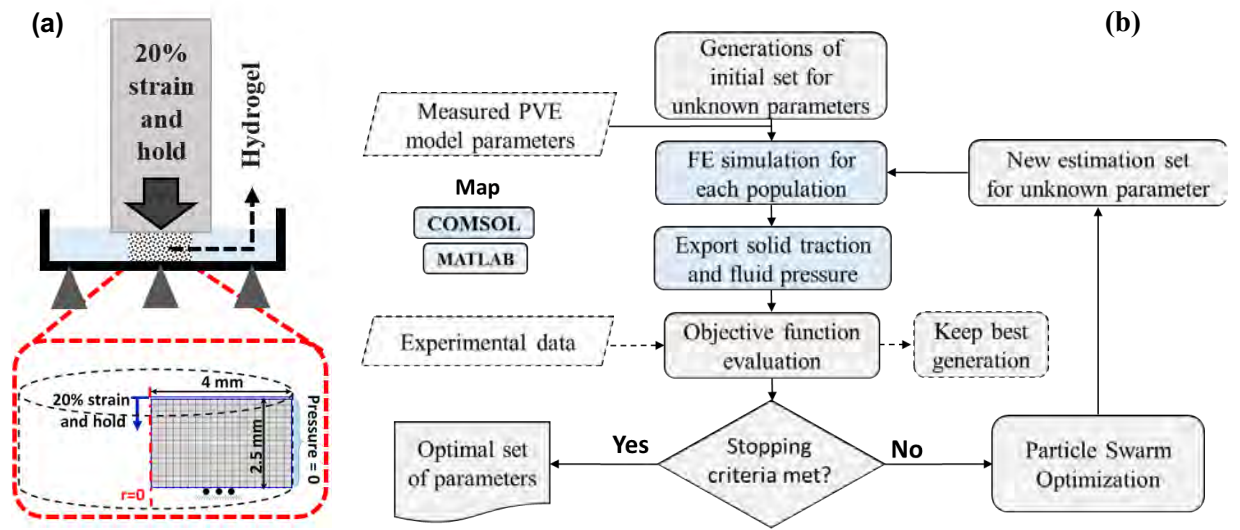
Figure S7. Emplyed method to separate flow-dependent and flow-independent load support via a poro-viscoelastic model. (a) Schematic of experimental setup and corresponding finie element model in COMSOL. (b) Flowchart of the combined experimental and computational methods for estimation of relaxation function parameters. The routine employes particle swarm optimization in MATLAB, and runs the finie element model iteratively to find the optimum set.

Table S3. Optimized relaxation time (τ_i) and modulus (G_i) of the PVE model relaxation function for the representative porous pHEMA hydrogels.

Porous hydrogel	G_1 (kPa)	τ_1 (s)	G_2 (kPa)	τ_2 (s)	G_3 (kPa)	τ_3 (s)	G_4 (kPa)	τ_4 (s)
8%Cr-Coarse	295e4	0.002	100	0.1	105	7.26	335	225
4%Cr-Fine	200	0.42	58	5.82	215	1600	-[a]	-[a]

a: It was not necessary to employ the fourth viscoelastic branch in Maxwell–Wiechert model (G_4 and τ_4) for the 4Cr-Fine hydrogel as we obtained good enough precision with n=3 on Prony Series for the relaxation function.

As can be observed in Figure S8-a and b, the optimized poro-viscoelastic model properly predicts experimental data and separates solid and fluid phases contribution (Figure S8-c and d). The obtained values to estimate the relaxation function by using the experiments, performed

at a 500 μm/s loading rate, were validated by comparing the model predication for another loading rate (e.g., 50 μm/s) with corresponding experimental data (Figure S8-e and f).
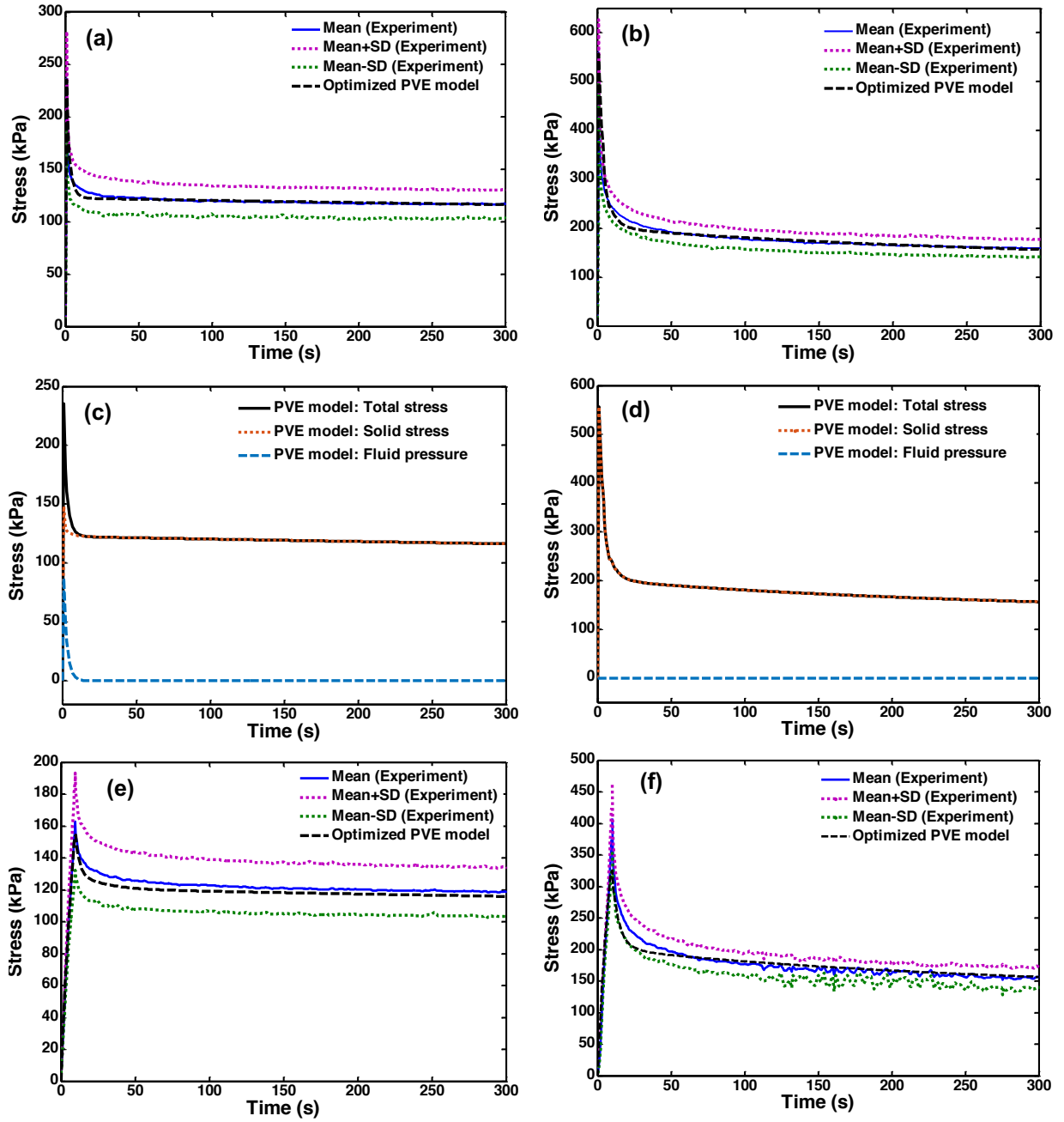

Figure S8. Separating flow-dependent and flow-independent load support by an optimized poro-viscoelastic (PVE) model. (a, c) 4Cr-Fine hydrogel experimental and simulation results for 500 μm/s loading rate. (b, d) 8Cr-Coarse hydrogel experimental and simulation results for 500 μm/s loading rates. (e, f) Validation of the developed poro-viscoelastic model in 50 μm/s loading for 4Cr-Fine (left) and 8Cr-Coarse (right) hydrogels.

Our simulation results revealed that the relaxation moduli (G_i) are directly correlated to the crosslinking density of the hydrogels, while there is an inverse correlation between relaxation times (τ_i) and crosslinking density of the polymeric network (Table S3). Moreover, the release of compression-induced fluid pressure takes a longer time in hydrogels with lower permeability

contrary to the instantaneous relief in highly permeable hydrogels. In this latter case, the total stress is sustained by the solid matrix (Figure S8-d) and this can be destructive for sample at maximum stress. On the other hand, the load is partly carried by the solid matrix at the maximum stress in the 4Cr-Fine hydrogel (Figure S8-c) owing to fluid pressurization as a result of its lower permeability.

Recoverability of hysteresis loop in porous hydrogels

The destructive and non-destructive processes contribution to the evolution of the porous hydrogels hysteresis loop was evaluated. In this regard, the level of energy dissipation over 100 cycles was compared between two loading sessions (10% static strain+10% dynamic strain at 1 Hz) performed with an overnight interval between them.
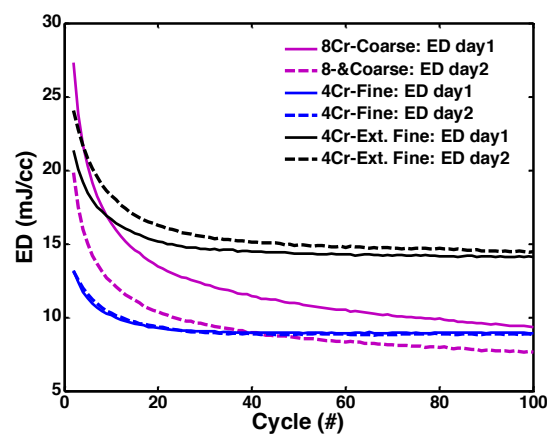

Figure S9. Typical hysteresis loop area (ED) variation for 8Cr-Coarse (purple), 4Cr-Fine (blue) and 4Cr-Extra Fine (black) during two cyclic loading tests performed with an overnight recovery time (the dissipation source in 8Cr-Coarse hydrogel is not recoverable indicating a destructive process).

The dramatic drop of ED in highly crosslinked sample (8Cr-Coarse) over loading cycles is partly due to the destructive sources of the energy dissipation (e.g., chains fracture or bond rupture during loading). After overnight resting, there is a partial recovery and the ED level (first cycle) for day 2, starts from a higher value than last cycle of the ED for day 1 as shown in Figure S9. However, this ED value is still lower than the first cycle of ED for day 1 (intact condition). In contrast, the combination of reversible solid intrinsic and frictional drag dissipations is fully recoverable in hybridly crosslinked and poorly permeable hydrogels (4Cr-Fine and Ext. Fine).

Cells distribution and viability in porous hydrogels

Human epiphyseal chondro-progenitor cells [8] were grown in standard incubator (37 °C and 5% CO_2) to 90% confluence, trypsinized and redistributed again in T75 culture flasks up to

passaged 5. The culture medium for cells during proliferation step was DMEM containing L-Glutamine, 4,5 g/l D-Glucose and Sodium pyruvate, (Life Technologies) which was supplemented with 10% FBS (Sigma) and 1% L-Glutamine and Penicillin (Life Technologies).

The 3-(4,5-dimethylthiazol-2-yl)-2,5-diphenyltetrazolium bromide (MTT) cell proliferation Kit I (Roche Corporation, Indianapolis, USA) was used to observe ECP cells distribution inside porous hydrogels. Knowing that permeability has a remarkable effect on cell seeding efficiency [3] and to balance initial population of cells in two groups, we used 1 and 1.3 million cells for seeding of 8Cr-Coarse and 4Cr-Fine hydrogels, respectively. After cell seeding, infiltration and distribution of cells were evaluated at day 2 by using a Stereomicroscope (LEICA MZ 16 1FA) following MTT staining as shown in Figure S10. Briefly, the cell-seeded hydrogels were cut in half and immersed in 300 ml DMEM medium (without phenol red) inside a 48 well plate. Then, 30 µl of MTT dye was added to each well and samples were incubated (37 °C and 5% CO_2) for 4 hours to let formazan formation. The insoluble purple formazan is produced due to cells metabolic activity and therefore demonstrates viable cells distribution within the hydrogels.
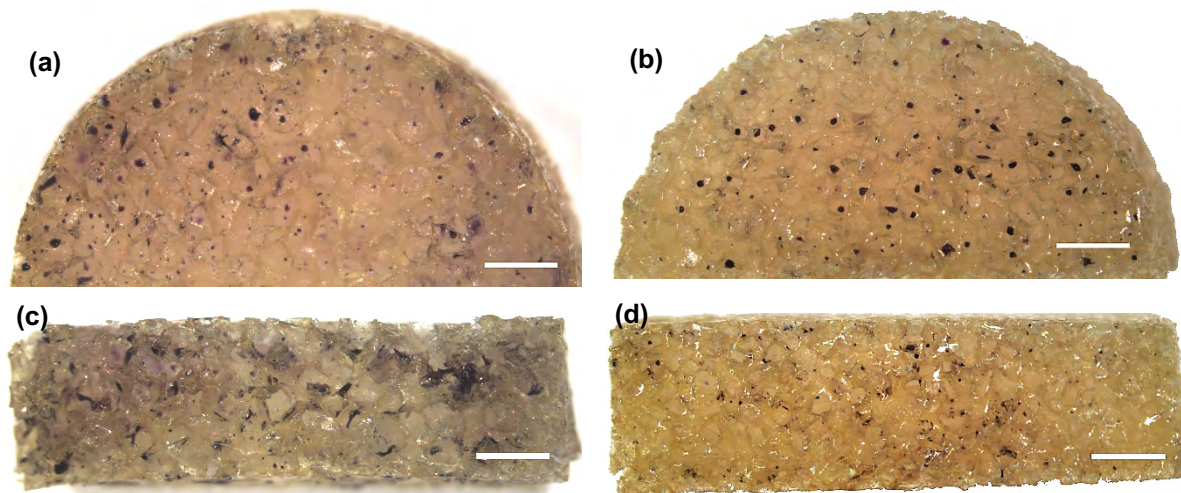

Figure S10. MTT stained cells distribution on surface and cross section of the porous hydrogels after 2 days. (a,c) 8Cr-Coarse porous hydrogel. (b,d) 4Cr-Fine porous hydrogel. The cells distribution and penetration are fairly uniform inside the hydrogels by employing customized CRIS seeding method we previously developed [3] (scale bar: 1 mm).

We also assessed the viability of the cells inside porous hydrogels (Figure S11) at different time points (day 5 & 10) by performing live and dead staining using Viability/Cytotoxicity Assay Kit (Biotium, Fremont, CA) following the manufacturer protocol. Before staining, the cell-hydrogel constructs were incubated in 1 ml DMEM medium without phenol red for 3 hours to diminish background color of the hydrogels due to phenol red in the proliferation medium. Then, the samples were stained by 500 µl of the mixed live/dead working solution (1 µl Calcein

and 2 µl Eht in 5 ml PBS) for 30 min at room temperature in dark. The samples were rinsed twice with PBS, and the images were taken by an invert LSM 700 confocal microscope (Carl Zeiss, Jena, Germany) using a 10X objective and subsequently processed with open source FIJI platform.
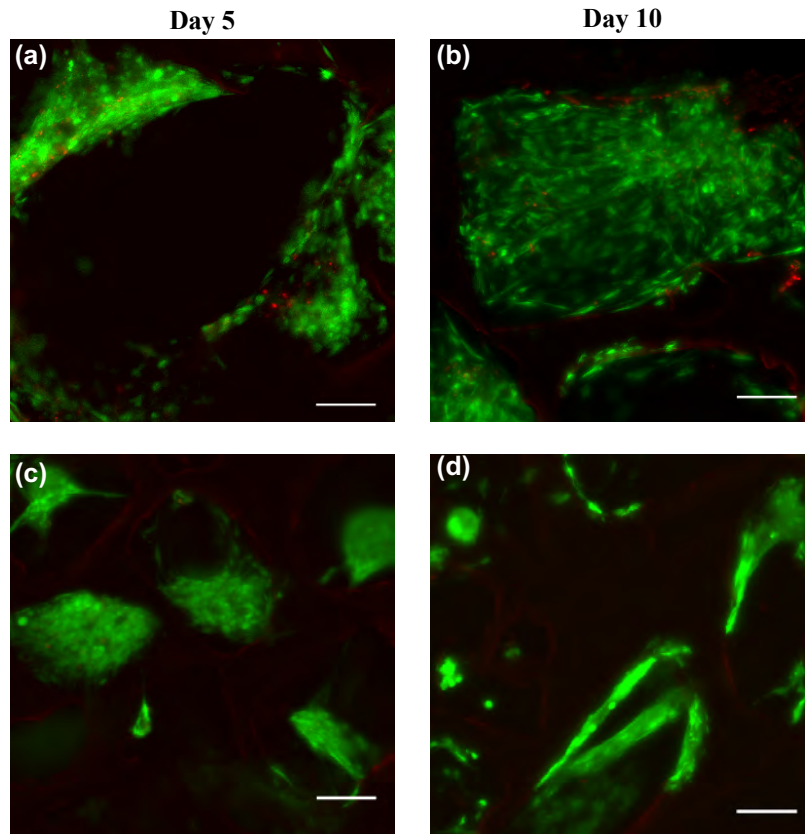
Day 5 **Day 10**

Figure S11. Live/dead staining of cells seeded porous hydrogels at different time points showing a stable cells viability up to 10 days of culture (scale bar: 100 µm). (a, b) 8Cr-Coarse. (c, d) 4Cr-Fine. Green stain illustrates live cells and red stain shows dead cells.

Mechanical stimulation of cell-laden hydrogels in cyclic compression mode

With the developed dissipative porous hydrogels, we studied the cells response to cyclic compression in a standard loading regime (10% cyclic strain over 10% static strain at 1 Hz). In the beginning of the 3D culture, the seeded hydrogels were pre-cultured for 3 days in proliferation medium inside a standard incubator (37°C, 5% CO_2). After this step, a differentiation medium was used and the mechanical stimulation was applied on the different groups of dissipative hydrogels (Figure S12-a). Differentiation medium was proliferation medium without FBS but having 10% ITS IV (Life Technologies) and 1% Vitamin C. We compared the expression of chondrogenic genes between the stimulated and non-stimulated groups of cell-seeded hydrogels.
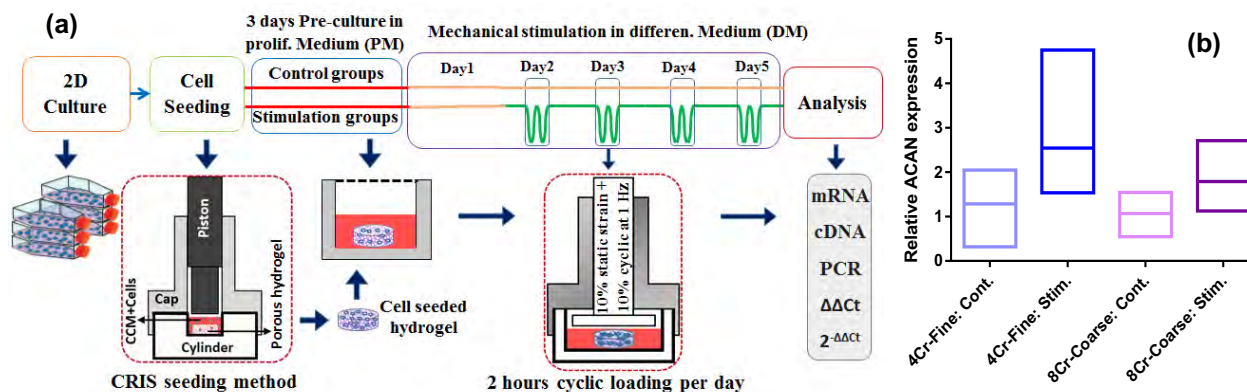
Figure S12. Performed *in vitro* mechanobiological experiment. (a) Schematic plan of the study. (b) Aggrecan (ACAN) gene expression shown as mean value with minimum and maximum ranges. Relative ACAN expressions are shown for two groups of dissipative hydrogel in free-swelling (control group) and mechanical stimulation (treatment group).

RNA extraction and gene expression

After the last period of stimulation in the mechanobiological experiment, each sample was put in a 2 ml Eppendorf tube containing 300 µl Trizol. Total RNA was extracted using the NucleoSpin® RNA (Macherey-Nagel) after a few steps of preparation [9]. Briefly, hydrogels were smashed by the polytron (Kinematica AG, Switzerland), while keeping the tube cold on dried ice. Then, 100 µl chloroform was added and centrifuged for 4 minutes at 12000 rpm at 4°C. The aqueous phase was transferred to 2 ml phase lock tubes and centrifuged for an additional 6 minutes at 12000 rpm. The aqueous phase was carefully transferred to 1.5 ml Eppendorf tubes and the extraction was completed by adding 5 µl RNA carrier and following the XS kit protocol. The RNA was quantified using the Nanodrop Lite Spectrophotometer (Thermo Scientific) and reverse transcription of 500 ng RNA was carried out for real time PCR analysis. Taqman® Reverse Transcription Reagents (Applied Biosystems) were utilized for cDNA synthesis in reaction volume of 50 µl containing master mix, random hexamer and RNA template.

Fast SYBR® Green Master Mix (Applied Biosystems) was used for PCR amplification in a final volume of 20 µl containing 1 µl of synthesized cDNA. Primers were synthesized by Microsynth (Balgach, Switzerland) according to reported sequences in Table S4. Different annealing temperature and concentration were used for primers to optimize the process resulting in efficiency range of 91 to 110%. The PCR amplification was carried out in duplicate for each sample by StepOnePlus Real-Time PCR platform (Applied Biosystems). The thermal cycling condition was defined as an initial 95°C step for 2 min followed by 40 cycles of 95°C

for 5s and corresponding annealing-extension temperature of gene (60 to 65°C, Table S4) for 30s. Gene expression data were analyzed using the comparative ΔΔCt method [10] with B2M as the reference gene. Corresponding free swelling hydrogels in each group were used as the biological reference for the stimulated hydrogels (n=4).

Table S4. Primers data used for qRT-PCR.

Gene	Anealing temp. (°C)	Primer concent. (nM)	Efficeny (%)	Sequence
COL2A	60	250	110	F: 5'- GGCAATAGCAGGTTCACGTACA-3' R: 5'- GATAACAGTCTTGCCCCACTTACC-3'
ACAN	62.5	200	91	F: 5'- GGTACCAGTGCACAGAGGGGTT-3' R: 5'- TGCAGGTGATCTGAGGCTCCTC-3'
SOX9	65	275	108	F: 5'-TGGAAACTTCAGTGGCGCGGA-3' R: 5'-AGAGCAAAAGTGGGGGCGCTT-3'
B2M	60	250	100	F: 5'- TATCCAGCGTACTCCAAAGATTCA-3' R: 5'- TGAAACCCAGACACATAGCAATTC-3'

Mechanical robustness of porous hydrogels subjected to large deformation

The structural stability of 4Cr-Fine versus 8Cr-Coarse porous hydrogels in large deformation was compared following the application of 70% compressive strain (twice) as shown in Figure S13.
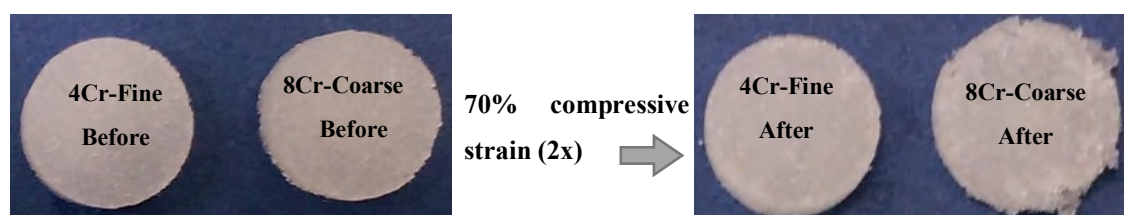

Figure S13. Structural stability of the 4Cr-Fine versus the 8Cr-Coarse porous hydrogels in large deformation. A plastic deformation and defects were observed in the 8Cr-Coarse hydrogel after 70% compressive strain, while the 4Cr-Fine hydrogel appropriately sustained the large deformation.

Supplemental References

[1] Peppas NA, Hilt JZ, Khademhosseini A, Langer R. Hydrogels in biology and medicine: from molecular principles to bionanotechnology. Adv Mater 2006;18:1345-60.

[2] Nasrollahzadeh N, Pioletti DP. Experimental method to characterize the strain dependent permeability of tissue engineering scaffolds. J Biomech 2016;49:3749-52.

[3] Nasrollahzadeh N, Applegate LA, Pioletti DP. Development of an Effective Cell Seeding Technique: Simulation, Implementation, and Analysis of Contributing Factors. Tissue Eng,Part C 2017;23:485-96.

[4] Suh J-K, DiSilvestro M. Biphasic poroviscoelastic behavior of hydrated biological soft tissue. Journal of Applied Mechanics 1999;66:528-35.

[5] Zahedmanesh H, Stoddart M, Lezuo P, Forkmann C, Wimmmer MA, Alini M, et al. Deciphering Mechanical Regulation of Chondrogenesis in Fibrin–Polyurethane Composite Scaffolds Enriched with Human Mesenchymal Stem Cells: A Dual Computational and Experimental Approach. Tissue Eng,Part A 2014;20:1197-212

[6] Marini F, Walczak B. Particle swarm optimization (PSO). A tutorial. Chemometrics Intellig Lab Syst 2015;149:153-65.

[7] Nasrollahzadeh, N; Pioletti, D P, Role of Flow dependent and flow independent viscoelasticity on time dependent behavior of visco-porous scaffolds. Proceeding of 15th International Symposium on Computer Methods in Biomechanics and Biomedical Engineering, Lisbon-Portugal, 2018.

[8] Darwiche, S.; Scaletta, C.; Raffoul, W.; Pioletti, D. P.; Applegate, L. A., Epiphyseal chondroprogenitors provide a stable cell source for cartilage cell therapy. *Cell Medicine* **2012,** *4* (1), 23-32.

[9] Abdel-Sayed P, Darwiche SE, Kettenberger U, Pioletti DP. The role of energy dissipation of polymeric scaffolds in the mechanobiological modulation of chondrogenic expression. Biomaterials 2014;35:1890-7.

[10] Livak KJ, Schmittgen TD. Analysis of relative gene expression data using real-time quantitative PCR and the $2^{-\Delta\Delta CT}$ method. methods 2001;25:402-8.